Aus der Poliklinik für Zahnärztliche Prothetik
Klinik der Universität München
Direktor: Prof. Dr. Daniel Edelhoff

Analysis of digitization methods for edentulous jaws

Dissertation
zum Erwerb des Doktorgrades der Zahnmedizin
an der Medizinischen Fakultät der
Ludwig-Maximilians-Universität zu München

vorgelegt von

Panagiotis Kontis

aus

Cholargos, Griechenland

Jahr

2023

Mit Genehmigung der Medizinischen Fakultät
der Universität München

Berichterstatter:	Prof. Dr. med. dent. Jan-Frederik Güth
Mitberichterstatter:	Prof. Dr. Karl-Heinz Kunzelmann
	Prof. Dr. Dr. Florian A. Probst
	Prof. Dr. Heinz Kniha
Mitbetreuung durch den promovierten Mitarbeiter:	PD Dr. med. dent. Christine Keul, M.Sc
Dekan:	Prof. Dr. med. Thomas Gudermann
Tag der mündlichen Prüfung:	25.05.2023

Table of Contents

1. Introduction

Despite constant improvements in public health and dental care over the past decades, complete edentulism still affects a surprisingly large number of patients, with a worldwide prevalence estimated between 4.0 and 4.9% [1]. In Germany, a recent study revealed that 12.4% of the population aged 64 to 75 years and 32.8% of the population aged 75 to 100 years suffer from total tooth loss. [2]. Hence, it is to be expected that the necessity for rehabilitation of edentulous patients will remain substantial in the coming decades [3].

The complete denture is the most common treatment method for edentulous jaws, in particular for patients where implant rehabilitation is not possible due to anatomical, medical, psychological, or economic factors [3]. Conversely, the established fabrication practices have remained essentially unchanged for the past 80 years, with well-known disadvantages [4].

Computer-aided design and computer-aided manufacturing (CAD/CAM) workflows have long been established in dentistry for the fabrication of fixed and partially removable prostheses [5], while recent innovations in digital design, virtual try-in, and material processing have expanded the advantages of digital dentures [6, 7]. Therefore, various manufacturers have already established systems for the digital fabrication of complete dentures [8].

Nevertheless, with most concepts, the first step of the fabrication process, meaning the acquisition of the patient’s jaw morphology, is achieved through digitization of conventional impressions or cast models with the use of extraoral scanners (EOS) [8]. Even though direct digitization with intraoral scanners (IOS) has demonstrated numerous benefits [9, 10] and sufficient accuracy in many clinical scenarios [11-13],

direct capture of edentulous anatomies remains limited [8]. Yet, the prospect of a fully digitalized process for complete denture manufacturing provides several advantages such as time efficiency, elimination of impression and model-related inaccuracies, reduced patient discomfort, archivability, and efficient communication between patient, dentist, and dental technician [14, 15].

Since the constant evolution of IOS technologies continues to improve the capabilities of the commercially available systems, further research should be focused on the accuracy of different digitization methods of edentulous jaws.

1.1 Conventional Approach

1.1.1 Conventional Workflow of Complete Denture Manufacture

The complete denture is one of the oldest treatment practices in dentistry with fabrication techniques that have been well established for the latter part of the past century [16]. Initially, preliminary impressions are taken, commonly with prefabricated impressions trays and irreversible hydrocolloid material (Alginate), and used for the manufacture of custom trays by the dental technician [17]. A second appointment is required for the acquisition of definitive impressions using the custom trays [18]. After the definite impressions have been poured with type IV gypsum to create master stone casts, bite registration plates with an acryl base and wax rims are prepared on the master casts [19]. In the next clinical appointment, the wax rims are adjusted corresponding to the maxillomandibular relationship (vertical and horizontal) of the future denture teeth. Facebow, vertical dimension, and centric relation are recorded using the rim plates along with the occlusal plane, lip line, smile line, canine line, and

facial midline [19]. Subsequently, the master casts are mounted using the facebow and centric relation on an articulator. The artificial denture teeth are set up with wax according to predetermined occlusion and aesthetic principles. In a later try-in appointment, the wax trial bases are placed in the patient's mouth so that the aesthetical, phonetical, and functional aspects may be evaluated. Adjustments can be carried out and depending on the extent of necessary changes subsequent appointments may be required. After the desired result has been achieved the wax trial bases are processed usually through injection, pouring, or packing and converted into acrylic. The finished dentures are reoccluded and polished before they can be inserted in the patient's mouth [19, 20]. Figure 1.1 depicts the clinical and laboratory steps of conventional denture fabrication.

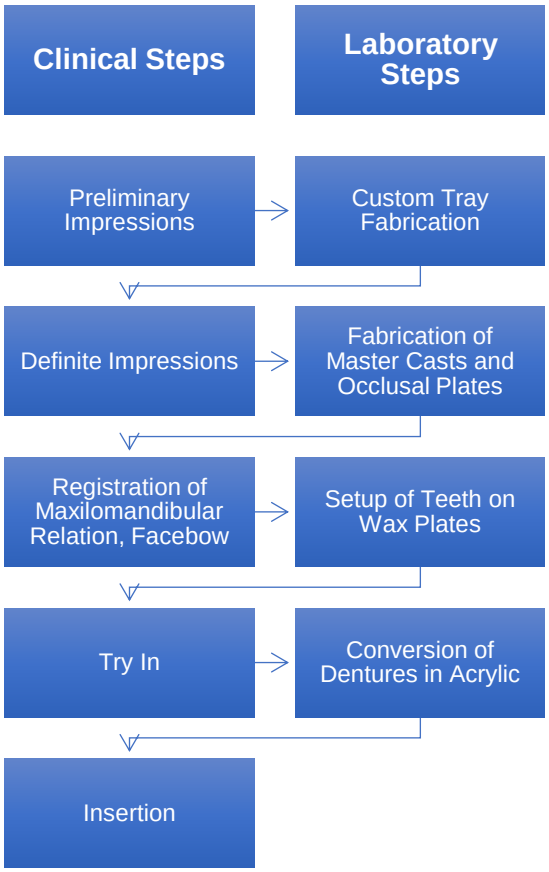

Figure 1.1: Clinical and laboratory steps of conventional denture fabrication.

Traditional workflows are associated with certain disadvantages including the substantial number of necessary appointments (at least five are required for the manufacture with additional post insertion adjustments), intensive and time-consuming laboratory work, and the resulting expenses [4].

1.1.2 Impression Technique

Impressions of edentulous jaws are considered particularly challenging. As the introductory step of the manufacturing procedure, impression taking is decisive in achieving the required retention, stability, and support for complete dentures. For that purpose, the junction between fixed gingiva and mobile mucosa needs to be truthfully captured during the movement of facial and masticatory muscles. This peripheral seal between the denture border and the surrounding soft tissue is necessary for maintaining a pressure gradient between the fluid film under the denture intaglio and the atmosphere [21-23]. Furthermore, an exact record of the edentulous anatomy, with minimal deformation of the highly resilient mucosal tissues ensures close contact of the denture base to the underlying structures and thus retention through cohesion, adhesion, and surface tension [21, 24].

Over the years a two-step protocol has been established for the impressions of edentulous jaws. Most methods involve the use of a custom tray manufactured after a preliminary anatomical impression [18-20, 25, 26]. The final functional impression is usually performed in two phases. The initial step requires border molding with a highly viscous thermoplastic material or high viscosity silicone while functional movements are performed by the patient (mouth narrowing and widening, adduction and lateral movement of the mandible, extension of the tongue, swallowing, Valsalva's maneuver, and pronunciation of the letter A) [17]. Subsequently, the mucosal bearing area is

recorded with a low viscosity impression material under the patient's performance of active functional movements [17]. In addition, several authors describe the reline of the vibrating line with wax on the upper edentulous jaw as the concluding step of impression making [17, 27, 28].

1.1.3 Impression Materials

A variety of diverse materials has been historically described for the definite impression of edentulous jaws including alginate, silicone, polyether, polysulfide, gypsum, and zinc-oxide eugenol [29]. In recent years, the popularity of elastomeric materials such as polyether and silicone has risen significantly due to their improved physical and mechanical properties [18, 30]. For this reason, only elastomeric impression materials will be discussed in the following segment.

1.1.3.1 Alginate

Alginate is an irreversible hydrocolloid. Alginates are sensitive to shrinkage caused by evaporation or swelling and therefore impressions must be poured immediately and can be poured only once [31]. Moreover, they exhibit very high hydrophilicity but minimal tear resistance [31]. Furthermore, polysaccharides inhibit the setting of gypsum, so pouring alginate impressions without prior treatment may cause deterioration in the quality of the casted model surface [32]. Alginate impressions are considered accurate enough for the fabrication of removable dentures but not for fixed restorations [31]. Primarily because of the low cost and ease of handling, alginates are some of the most popular materials for edentulous jaw impressions [29].

1.1.3.2 Silicone

Silicones can be divided into two subgroups, condensation crosslinking silicones, and addition cross-linking silicones. Condensation crosslinking silicones require a polycondensation reaction between terminal hydroxyl-groups of the silicone pre-polymers and alkyl silicate catalyzed by dibutyl-tin dilaurate to form a three-dimensional network in a condensation reaction. By-products of the reaction such as ethyl alcohol eventually escape through evaporation resulting in an overall contraction of the impression [31-33]. Condensation crosslinking silicones produce precise impressions if poured quickly after setting, but suffer a substantial polymerization shrinkage with time and may cause allergic reactions due to mucosal contact with the catalyst [32, 34]. By contrast, addition crosslinking silicone – polyvinyl siloxane (PVS) or vinyl polysiloxane (VPS) – solidify through an addition reaction between divinylpolysiloxane and polymethylhydrosiloxane in the presence of a platinum salt catalyst (Figure 1.2). This reaction produces no by-products and consequently a lesser extent of shrinkage, although the subsequent reaction of platinum with water or hydroxyl groups may release hydrogen gas causing voids in the gypsum casts [32, 33].

The numerous advantages of addition silicones, namely excellent depiction of clinical details, high elastic recovery (99%) and detail reproducibility, dimensional stability, low toxicity, and better patient acceptance render them the impression material of choice for many practitioners [34-36]. Furthermore, addition silicones have time and again demonstrated superior accuracy to condensation silicones [34, 37, 38].

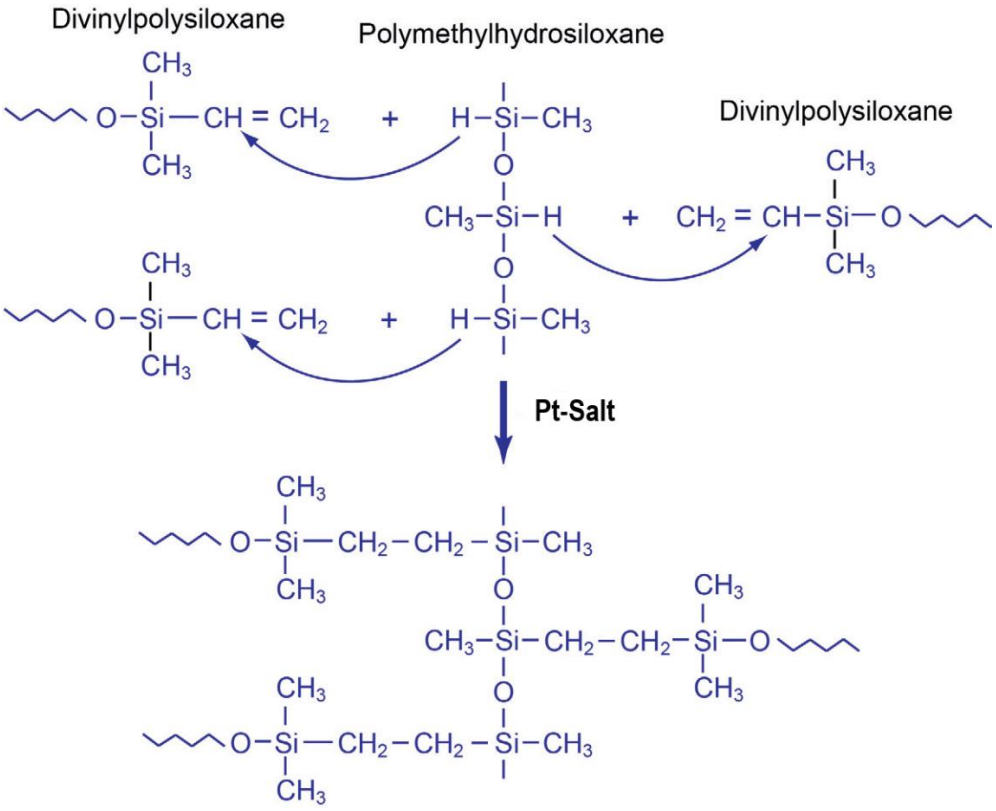

Figure 1.2: Polymerization of Polyvinyl Siloxane (PVS) [32].

A significant disadvantage of silicone lies in the hydrophobic nature of the material since, in most instances of intraoral use, contact with saliva, blood, or hydrophilic surfaces (dentin) is unavoidable. To this extent, manufacturers attempt to increase the hydrophilicity of the material through the addition of nonionic surfactants [32]. These amphiphilic surfactant molecules aggregate on the surface of the impression after setting and can diffuse from the PVS into the aqueous phase and thusly reduce the surface tension. This results in a more wettable surface and therefore fewer voids in gypsum casts [32, 36]. Nevertheless, adequate control of the circumjacent moisture is paramount for the achievement of clinically acceptable impression [31]. A further limitation regarding the use of addition silicones is the inhibition of polymerization through interaction with diverse materials such as hemostatic solutions, metal ions,

sulfides of latex gloves or dental dams, and even methacrylate composite residues from core build-up [36].

Regarding impressions of edentulous jaws, a significant advantage of PVS is the availability of a wide variety of viscosity pastes, which can be combined for border molding and recording of the denture base depending on the degree of required tissue compression [36]. At the same time, PVS materials allow for a corrective impression [39]. A recent study reported no differences in the accuracy of polyvinyl-siloxane, polysulfide, and polyether impressions of the edentulous maxilla in vitro [40].

1.1.3.3 Polyether

Polyethers were first introduced in the market in the late 1960s and have since been elevated to one of the most widely used impression materials. Polyether produces impressions with excellent accuracy, very high detail reproduction, and exquisite dimensional stability for up to one week [29, 32]. Moreover, polyether is considered hydrophilic due to the presence of carbonyl (C=O) and ether (C-O-C) groups and therefore thought to perform better in wet environments such as subgingival areas, mucosa, and moist teeth [31, 36, 41, 42]. Disadvantages of polyether include the unpleasant taste, relatively high cytotoxicity compared to other impression materials, and high rigidity, which may result in difficulty in removing the impression from the patient’s mouth or poured stone casts [32, 36]. Polyether has been theorized to be more compatible with the inherent moisture of the mucosal tissues because of its hydrophilic nature and therefore better suitable for capturing the edentulous anatomy [18, 29]. On the other hand, correctional impressions are not possible with most polyether materials.

1.1.3.4 Polyvinyl Ether Silicones

Polyvinyl ether silicones (PVES) materials are a combination of polyvinyl siloxanes and polyether and incorporate properties from both material classes. They are more hydrophilic than PVS, have high elastic recovery, dimensional stability, and tear resistance [43]. Additionally, their accuracy is on par with that of polyether and PVS.

1.1.3.5 Polysulfides

Polysulfides are polymers that contain multifunctional mercaptan (-SH) groups and solidify by condensation polymerization reaction between the -SH groups and oxygen from the lead oxide catalyst [32]. Polysulfides show moderate hydrophilicity, good tear strength, but low rigidity and elastic recovery [31]. However, as polysulfides do not adhere to themselves, they cannot be used for correctable impression or shaping of the peripheral seal [36].

1.1.3.6 Impression Compound

Impression compound is a thermoplastic material that usually consists of a blend of waxes, thermoplastic resins, and a coloring agent, most commonly shaped as sheet and sticks. When heated above its fusion temperature the compound becomes soft and can be deformed to adapt to and capture the intraoral anatomy [32]. After cooling the material becomes rigid and retains its form [32]. These characteristics render impression compound ideal for border molding as it can be placed at the edge of the custom tray and closely adapted to the vestibule [18].

1.2 Computer-Aided Approach

1.2.1 Historical Background

Historically, the first concept of computer-aided manufacturing for complete dentures was introduced in 1994 by Maeda et al. who described the fabrication of complete dentures with rapid prototyping of polymerized composite resin [44]. After that, Kawahata et al. proposed a method for the duplication of existing dentures through milling [45]. A decade later the first papers explicating the digitization of edentulous casts and the use of computer-aided design for the arrangement of teeth followed by conventional manufacturing techniques were published [46, 47]. Zhang et al. developed a prototype of a robotic multimanipulator tooth-arrangement system in 2011 [48]. Other authors explored the possibility of virtual tooth arrangement combined with computer numerical control (CNC) milled denture bases and manual placement of the teeth into recesses of the base [49, 50]. Inokoshi et al. developed the first protocol for rapid prototyping fabrication of a digitally designed trial and concluded it to be similarly accurate to a conventional trial [51]. Belgin et al. described the fabrication of denture teeth with CAD/CAM and additive manufacturing technologies, which were afterward placed on wax rims and incorporated into the prostheses through conventional methods [52]. Recently, the integration of innovative concepts and technologies, in particular, the virtual articulator and face scan further elevated the status of CAD/CAM complete denture through the reduction in treatment time, laboratory work, cost, and improved predictability of treatment outcome [4, 53, 54].

1.2.2 CAD/CAM Workflow of Complete Denture Manufacture

Nowadays, several protocols have been developed by numerous manufacturers to increase the involvement of CAD/CAM technologies in the conventional fabrication chain of complete dentures [6, 8, 55]. Generally, CAD/CAM manufacturing of complete dentures requires a digital dataset of the edentulous anatomy. This dataset can be obtained through indirect digitization of a conventional impression or stone cast or direct digitization with an IOS [55]. A maxillomandibular relationship record is necessary for the orientation of the datasets in the design software. Currently, this step has to be achieved with conventional or 3D-printed baseplates supporting wax occlusion rims [55]. The data is imported into specialized software. Teeth are selected from a variety of libraries or individually modeled. Digital arrangement of teeth and design of denture base can be conducted, while analysis of the static and dynamic occlusion is possible through the virtual articulator [53]. A virtual setup with the use of face scanning technology facilitates the evaluation of tooth position, shape, and size [4, 54]. Try in templates with acrylic or wax rims can be milled or printed and allow the assessment of the setup in a clinical appointment [8]. The definitive denture can be manufactured subtractively through milling of prepolymerized resin discs (monolithic dentures or milled denture base with bonded teeth) or additively (rapid prototyping) [8, 55].

1.2.3 Advantages

Significant research has been conducted regarding the advantages of CAD/CAM complete dentures versus conventional dentures. Generally, computer-assisted workflow is associated with time efficiency, reduced number of appointments, less clinical chair time, shorter and fewer laboratory steps, and reduced costs [56].

Furthermore, digital data are stored, archived, and are readily available in case a replacement denture or a surgical/radiographic guide is needed [7, 8]. Dentures fabricated from pre-polymerized CAD/CAM acrylic resin exhibit superior dimensional stability and fit and have been therefore theorized to provide improved retention compared to conventional dentures [57-59]. These claims could be supported by clinical investigations that demonstrated increased retention for CAD/CAM dentures [60, 61]. Moreover, improved physical properties such as higher elastic modulus, flexural strength, and fracture toughness allow the fabrication of dentures with lower minimal thickness and thusly positively affect patient acceptance [62]. In addition, milled dentures have been described as more biocompatible since they release less residual monomer and are more resistant to bacterial adhesion [63, 64]. On the other hand, the steep learning curve and environmental impact of the techniques have been discussed as possible disadvantages [8].

1.2.4 Digitization

The first step of any computer-aided workflow is the generation of a model dataset of the intraoral anatomy, which is thereafter used to design and manufacture a prosthesis using CAD/CAM software. This dataset can be acquired through indirect digitization of conventionally generated impressions or master casts by a laboratory scanning device or by direct digitization of the jaw with the use of an intraoral scanner (IOS) [54]. Almost exclusively, CAD/CAM workflows for complete dentures rely on extraoral digitization of functional impressions or master casts for data acquisition [55], although the recent advances and increased popularity of IOS have given rise to consideration of their possible use in completely edentulous situations [54].

1.2.4.1 Indirect Digitization

The method of indirect digitization represents a semi-conventional workflow. The intraoral anatomy is captured through a conventional impression, which can be poured with gypsum. A laboratory extraoral scanner (EOS) is used to scan the impression itself or the plaster model [65]. Most laboratory scanners employ optical measurement methods such as active confocal microscopy and active optical triangulation (In Eos X5, D800 3Shape), although some devices also work with mechanical measuring methods [66].

EOS operate under controlled conditions of temperature, light, humidity, with a highly automated process and unlike IOS are not affected by the limitations of direct digitization such as patient movement, presence of saliva or blood, subgingival margins, and scanning strategy [11]. However, the accuracy and quality of optically based EOS diminish when long and deep hollow spaces and undercuts or highly reflective surfaces are scanned, particularly for impression digitization [67]. For this reason, several manufacturers have developed scannable impression materials. Furthermore, with indirect digitization errors inherent to the conventional procedures namely, contraction and deformation of the impression and expansion of the stone cast still affect the accuracy of the final dataset [68].

1.2.4.2 Direct Digitization

Direct digitization with IOS has become the cornerstone of the fully digitized CAD/CAM workflow with its numerous advantages already extensively discussed in the literature. These include time efficiency, reduction of patient discomfort, simplification of clinical procedures, facilitated archiving, improvement of communication with the patient and dental technician, color reproduction, chairside analysis of the performed

preparations, savings in conventional materials [9, 10, 14, 15]. Nevertheless, IOS do present certain disadvantages such as a steep learning curve, a significant financial investment, insufficient simulation of dynamic occlusion, difficulty in detecting deep marginal lines of prepared teeth, and unreliable accuracy regarding complete arch digitization [9, 10, 15].

To date, a plethora of indications for IOS are advertised by various manufacturers in almost every field in dentistry including prosthodontics, implantology, and orthodontics. Clinical applications for the use of IOS are the manufacturing of fixed single and multiple tooth or even implant-supported restorations, removable partial dentures, surgical guides, mouth guards, orthodontic appliances, dental models, and even determination of tooth color and shade [10, 15]. Still, most of these claims lack the necessary research to be proven accurate and feasible alternatives to the conventional approach.

Essentially, numerous successive images are captured with the use of an intraoral camera and overlapped by dedicated software to produce the digital model [69]. With increasing number of acquired images, minute discrepancies in image arrangement accumulate and result in inaccuracies in the dataset [70]. This superimposition error is thought to be contingent on a number of factors including the optical technology, size and number of captured images, iteration algorithm, scanning strategy, distinctiveness of the captured surface, and operator experience [71].

1.2.4.3 Scanning Principles

A variety of noncontact, reflective optical technologies such as confocal microscopy, optical coherence tomography, active and passive stereovision, triangulation, active wavefront sampling, interferometry, and phase shift principles are utilized by EOS and IOS for the capture of the intraoral anatomy [65]. Because of their relevance to the

systems employed in the current study the principles of active confocal microscopy, active optical triangulation, and active wavefront sampling will be further discussed in the following paragraphs.

1.2.4.3.1 Active confocal microscopy:

Confocal laser beams are generated, meaning that the emitted laser beam and the reflected laser beam are superimposed. The emitted laser beam is focused by a lens and then impinges at the object on a narrow focal point with a shallow depth of field. The beam is then reflected by the object, bundled again by the lens and a part of it is redirected by a beam splitter. The redirected light reaches a diaphragm, which eliminates beams originating outside the focal point. The light beam is converted into an electrical signal by a photodetector and since the focal length is known, the distance to the recorded object point can be determined (Figure 1.3).

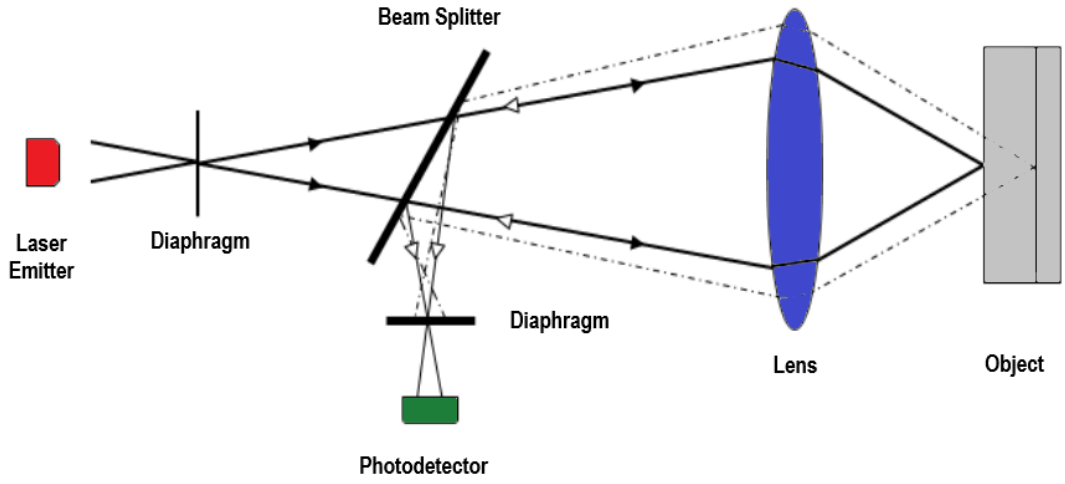

Figure 1.3: Simplified illustration of the Active Confocal Microscopy principle. Own representation based on [65].

The focal point is moved horizontally with the help of adjustable beam displacers or mirrors and vertically by raising or lowering the lens to capture more images of the object [65, 72]. This method picks up individual points from a certain depth and then connects them, creating a three-dimensional dataset from the recorded two-dimensional images [14].

Parallel confocal microscopy facilitates powder-free scanning and the capture of colored images. The handpieces of the IOS are usually somewhat larger to contain the complex lens and laser systems needed to preprocess a large amount of data [73]. In the current study, iTero Element (Align Technology) and Trios 3 wireless (3Shape) operate with active confocal microscopy.

1.2.4.3.2 Active optical triangulation:

With active optical triangulation, a light beam is emitted by a laser and subsequently deflected by a mirror at a known angle. The beam then reaches an object and is reflected. The light that reaches back into the scanning head is collected via a lens and directed to a charge-coupled device (CCD) or complementary metal-oxide-semiconductor (CMOS) sensor. As laser beams from different points of the object are gathered, a dot pattern contingent on the geometry of the scanned object is composed on the sensor's field of view. In essence, a triangle between laser, sensor, and reflection point is formed (Figure 1.4).

Since the distance (d) of laser to the sensor and the angle of deflection of the laser beam (α) are known and the angle of reflection on the object (β) can be calculated, the distance of each scanned point and the sensor can be determined through trigonometric equations [14]. Thusly, each scanned point can be assigned X-, Y- and Z- coordinates [65]. To accelerate the image acquisition of large areas, light patterns such as stripes or grids are projected onto the object.

A limitation of active optical triangulation is the difficulty and sometimes inability to record undercuts. Because of the firmly defined angle between the light source and the sensor certain undercut areas cannot be accessed by either the laser source, the sensor, or both. Reduction of the triangulation angle could alleviate this problem but would lead to a decrease in accuracy. Accuracy is also negatively affected with increasing distance from the lens to the sensor and from the laser source to the sensor [74]. However, these parameters are limited by the acceptable size of the scanning head [65]. Moreover, accuracy can be influenced by the reflective properties of the scanned surface, therefore some authors propose the use of a coating powder to achieve a uniformly reflecting surface, although recent systems do not require powdering to reliably capture surfaces [14]. In the current study, active optical triangulation is employed by the Cerec AC Omnicam (Sirona Dental Systems).

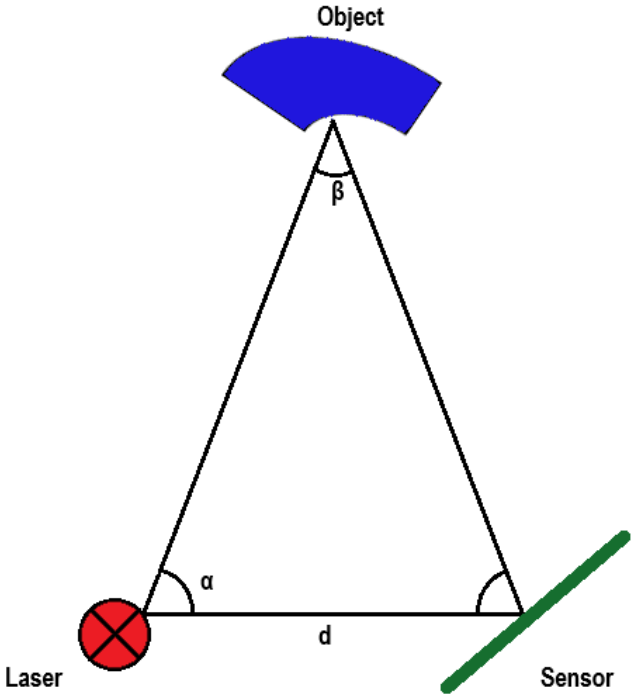

Figure 1.4: Simplified illustration of the Active Optical Triangulation principle. Own representation based on [75].

1.2.4.3.3 Active wavefront sampling:

Systems based on active wavefront sampling (AWS) technology operate using a camera in conjunction with an AWS module. This AWS module is essentially a decentralized aperture that rotates around the optical axis. Only light that passes through the opening reaches the camera at any given time producing a circular array of target points on the image plane [73]. The distance between the focal plane and object can be derived through algebraic formulas when the diameter of rotation of a point on the image plane is known. The use of a single aperture results in higher spatial resolution [65]. A simplified illustration of the principle is depicted in Figure 1.5. Current IOS on the market which employ the wavefront sampling technology require a stochastic pattern of reference points to match video recordings. Therefore, powdering with TiO_2 (titanium dioxide) prior to scanning is necessary. In the current study, active wavefront sampling is employed by the True Definition Scanner (3M Deutschland GmbH).

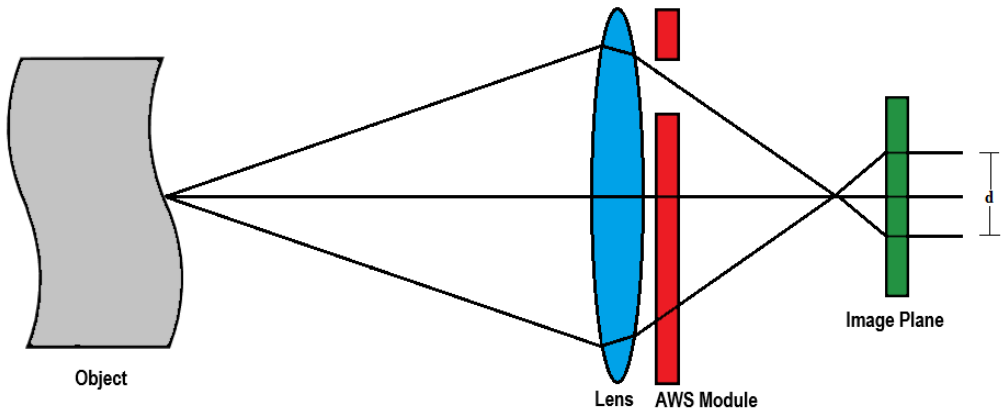

Figure 1.5: Simplified illustration of the Active Wavefront Sampling principle. Own representation based on [75].

1.2.4.4 Scanning Strategy

Scanning strategy has been extensively discussed as a factor that can significantly affect the quality and accuracy of the generated dataset [71, 76, 77]. Ender et al. reported differing accuracies when comparing six scanning strategies for Lava C.O.S, Cerec Bluecam, and Cadent iTero [78], while Medina et al. found iTero to be significantly affected by diverse scanning strategies [79]. Passos et al. deduced that a continuous scanning path starting with the palatal, moving to the occlusal, and concluding with the facial surface of the maxillary teeth to be most true with the Cerec Primescan and Omnicam systems [80].

In the absence of consensus on the optimal scanning strategy, most researchers rely on the manufacturer's recommendation for each system regarding scanning protocols [81]. In a recent investigation, the recommended scanning pattern (first capture of the occlusal-palatal surfaces and then the occlusal-buccal side of the arch) for Trios 3 was determined to be the most accurate [82]. Di Fiore et al. concluded that tilting of the scanning head from occlusal to lingual and back to buccal while scanning the arch, as per manufacturer's suggestion, produced the best results on an edentulous mandible model in vitro [83].

Nevertheless, research involving scanning protocols on edentulous jaws seems to be limited. Furthermore, most proposed scanning strategies apply only to dentate situations. Completely edentulous jaws have been theorized to be more challenging to accurately capture because they lack anatomical landmarks used as reference by the IOS's algorithm for image overlap [84]. To the author's knowledge, only one study has compared different scanning strategies on an edentulous maxilla in vitro [85]. This investigation suggested a scanning path commencing on the ridge top of the edentulous arch moving from one tuberosity to the other, proceeding with the capture

of the buccal side of the edentulous ridge and concluding with the palate. Moreover, several authors have proposed the placement of artificial reference structures to facilitate intraoral scanning of edentulous ridges [86-88].

1.3 Review of Literature

Over the past decades, significant research has been conducted regarding the use and applicability of IOS. Although initial reports demonstrated the challenges of direct digitization [72, 89], recent research indicates similar and even superior accuracy for IOS compared to conventional impressions regarding restorations with the span up to one quadrant [12, 90]. Meanwhile, direct digitization of full arches has been shown to produce clinically acceptable accuracy [13, 91, 92]. Despite the prevalence of complete edentulism in elderly patients and increasing incorporation of direct digitization in the routine of everyday practice, intraoral scanning with IOS is almost exclusively applied to data acquisition of tooth or implant-supported, fixed restorations, and recording partially edentulous anatomies [93]. The digitization of edentulous anatomies presents primarily three limitations: the lack of anatomical landmarks, the functional borders, and the posterior palatal seal [55, 94]. Generally, scanning of edentulous arches is considered to be less accurate than the digitization of dentate situations, since the scarcity of reference features results in insufficient overlap of the captured images by the software algorithm and therefore diminished accuracy of the generated dataset [84, 95-98]. Workflows involving direct digitization with IOS in combination with further CAD/CAM technologies for the manufacture of complete dentures in a clinical setting have already been described, although researchers have pointed out existing challenges [54, 99-103].

Patzelt et al. were the first to assess the possibility of direct digitization of edentulous jaws in vitro and discommended the use of IOS in vivo [84]. Another in vitro study reported high accuracy (maximal deviations of 51µm) for the digitization of edentulous jaws with Cerec Primescan [104]. Tasaka et al. simulated the viscoelastic properties of the mucosa on a model with artificial mucosa and measured IOS's error equal or lower to the extent of tissue displacement [105]. Osnes et al. compared the precision of six IOS on an edentulous maxillary model and found Trios 3, Cerec Omnicam, True Definition Scanner, and Aadva iOS 100 to be within the clinically acceptable range [106]. Only one investigation evaluated the accuracy of five IOS on edentulous ridges by comparing the distances between cylindrical markers in vitro [95].

Previous in vivo comparisons of direct digitization with IOS versus indirect digitization of impressions or stone casts of edentulous arches found no significant differences [107-109]. Lo Russo et al. concluded no significant differences between IOS and impression digitization since the reported differences were attributed to mucosal resilience [108]. Chebib et al. reported similar deviations for the digitization with Trios 3 and scanned PVS impressions over the entire maxilla, although inspection of local deviations revealed lower trueness for direct digitization at the peripheral border and inner seal [109]. Ex vivo digitization of an edentulous cadaver maxilla revealed lower accuracy for Medit i500 compared to iTero, Cerec Primescan, Trios 3, and Trios 4, although all systems were deemed clinically accurate [110]. By contrast, Hack et al. reported significant differences between IOS and digitized impressions and casts with aberrations above the threshold of clinical importance (500µm) primarily in areas of non-attached tissues [93]. In another investigation, IOS produced higher discrepancies to digitized stone casts in the buccal vestibule of the maxilla, buccal and lingual vestibules, buccal shelves of bone, and retromolar pad areas of the mandible

and were therefore not recommended for the digitization of edentulous arches [111]. A recent comparison of 3 IOS based on digitized preliminary impressions found similar trueness for Cerec Primescan, Trios 3, and Medit i500 [112]. Generally, significant differences between intraoral scans and extraoral digitization seem to be more frequent and pronounced in areas of flexible soft tissues such as the vestibular and lingual sulci, while the non-mobile structures with higher resilience display lower deviations [113].

The vast majority of in vivo and in vitro examinations describe accuracy through differences between surface points of datasets after best fit superimposition [113]. However, best fit superimposition arranges the datasets as closely as possible, which has been proven to result in underestimation of the actual inaccuracy [114]. Moreover, discrepancies caused by the iterative algorithm may influence the results, especially considering larger datasets [115]. Alternatively, comparisons on the basis of reference geometries (spheres, metal bars, scan bodies) placed on either completely dentate or edentulous arches may mitigate some of the issues associated with best fit comparisons [11, 69, 116-118]. However, the required very highly accurate dataset of the intraoral anatomy is difficult to achieve, in particular for edentulous situations [11].

2. Aim of the study

The present study aims to evaluate the accuracy (trueness and precision) of direct digitization, using IOS, and indirect digitization of conventional PVS impressions and plaster cast models using EOS, in terms of distance and angle aberrations on an edentulous maxillary model. The outline of the study is depicted in Figure 2.1.

The null hypothesis was that there are no differences in the accuracy of the model datasets between the different digitization methods of an edentulous upper jaw model.

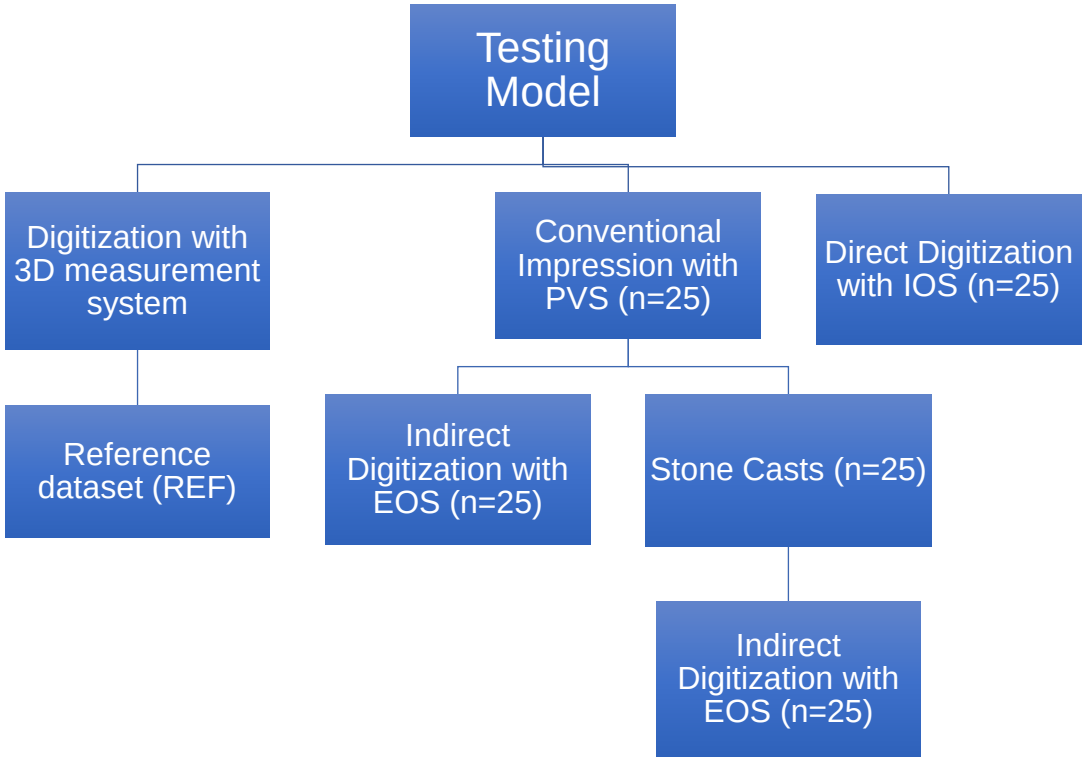

Figure 2.1: Outline of the study.

3. Materials and Methods

3.1 Testing Model

An edentulous resin model of the upper jaw (B-3NM Frasaco GmbH, Tettnag, Germany) was digitized using the S600 ARTI dental laboratory scanner (Zirkonzahn GmbH, Gais, Italy). The generated STL (surface tessellation language) data were imported into metrological software (Control 2015, Version 2015.1.0.1919, Geomagic, Morrisville, MC, US). A construction dataset was generated by attaching four hemispheres of identical dimensions were to the alveolar ridge in the area of the canines and the second molars. Based on the construction dataset, a model was milled from PEEK (Polyether ether ketone) (PEEK Biosolution, LOT no 32116; Merz Dental GmbH, Lütjenberg, Germany) using the M5 Heavy Metal Milling Unit (Zirkonzahn GmbH) and used as the testing model for the present study (Figure 3.1).

Figure 3.1: Testing model milled from PEEK [119].

A reference dataset (REF) (Figure 3.2) was obtained after digitization of the testing model with an optical 3D measurement system (InfiniteFocusG5; Alicona Imaging GmbH; Graz; Austria; objective 5x, resolution: finest topographic lateral = 3.51 µm, vertical = 410 nm) and afterward imported into the software control 2015.

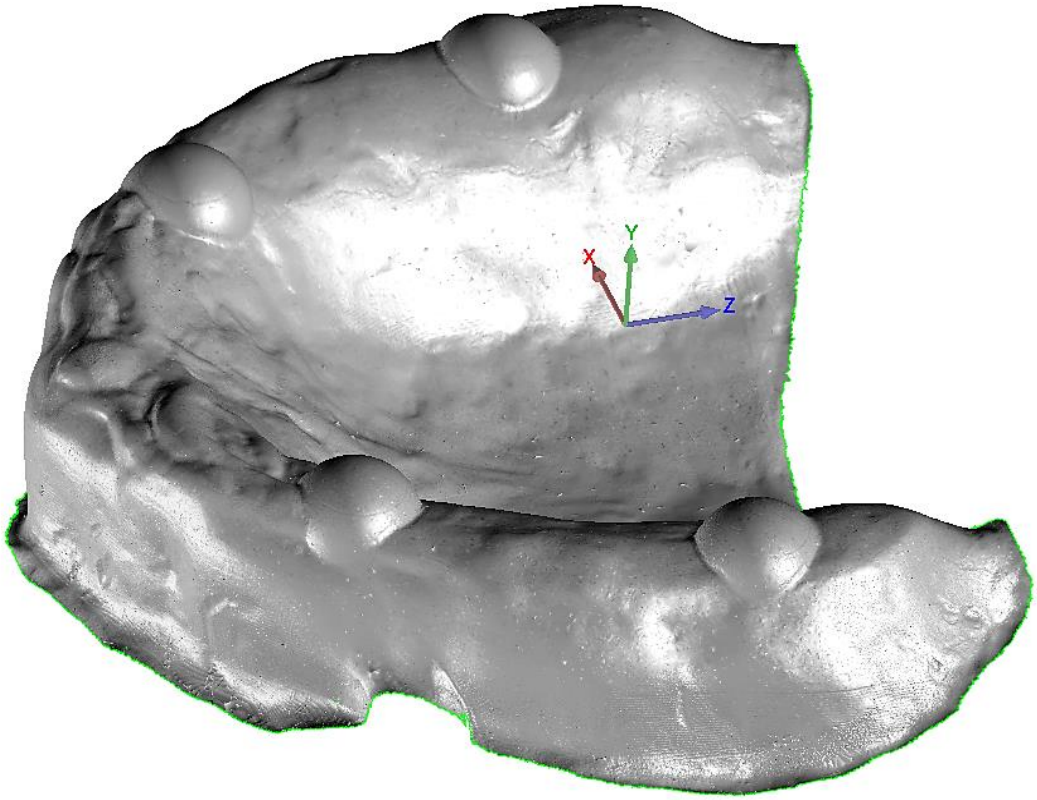

Figure 3.2: REF introduced in the coordinate system. XY-plane and XZ-plane depict the frontal and transverse planes respectively. The Y-axis represents the vertical direction [119].

3.2 Direct Digitization

The PEEK testing model was digitized with five IOS (n=25/group):

- Cerec Primescan AC (Group PRI; Software version 5.0.2, Dentsply Sirona, Bensheim, Germany)
- Trios 3 Wireless (Group TRS; Software version 1.4.7.4, 3 Shape, Copenhagen, Denmark)

- True Definition Scanner (Group TRD; Software version 5.3.1 – “Production-eu“, 3M, Seefeld, Germany)
- iTero Element (Group ITE; Software version 5.7.0.293, Align Technology, San Jose, California, United States)
- Cerec AC Omnicam (Group OMN; Software version 4.5.2, Dentsply Sirona, Bensheim, Germany)

Each scanning session with Cerec Primescan AC, Trios 3, and Cerec AC Omnicam was initiated with the calibration of the device according to the manufacturer's recommendations. Prior to the scanning process with the True Definition scanner, a TiO_2 coating (Lava Scan Powder, LOT no N203051, 3M) was applied. None of the other devices required powdering.

All scans were conducted within the span of twenty days, in the same room, with a five-minute recess between each scan, by one single trained user according to manufacturers´ specifications. The following strategy was applied with each intraoral scanner: scans were initiated at the maxillary tuber of the first quadrant. The vestibular surface of the alveolar ridge was first recorded. After that, the palatal side of the alveolar ridge from the second to the first quadrant was digitized. Scanning concluded with the capture of the palate in a zigzag motion.

The test datasets were post-processed and exported as STL from the Cerec Primescan AC, Cerec AC Omnicam, Trios 3 Wireless, and the EOS. In the case of the True Definition and iTero systems, the test datasets were sent to the manufacturers´ data processing center, post-processed, and exported as STL after return.

3.3 Indirect Digitization

Twenty five conventional impressions of the testing model were taken (Figure 3.3). Scannable PVS impression material (Flexitime Fast&Scan light flow, LOT no K010022 and Flexitime Monophase Pro Scan, LOT no R010022; Kulzer GmbH, Hanau, Germany) and light-cured anatomical custom impression (Palatray XL, LOT no A0984; Kulzer GmbH) trays were used. The individual trays were designed with a 3 mm spacer on the anterior and posterior parts of the alveolar ridge, to ensure positional stability of the tray and adequate thickness of the impression material. The custom trays were manufactured twenty-four hours prior to taking the conventional impressions. During impression taking, light body material (Flexitime light flow) was applied around the hemispheres, the tray was loaded with medium body material (Flexitime Monophase), and then positioned and held without pressure. The impression was removed from the PEEK model after four minutes, placed in a disinfection bath (ORBI-Sept Abformdesinfektion, LOT no A0984; Orbis Dental, Münster, Germany) for two minutes, and subsequently cleaned under running water and air-dried.

Following a twenty-four-hour storing period in a room with a temperature of 18 ± 1 °C, relative humidity of 72 ± 3%, and air pressure of 764 ± 5 mmHg, STL datasets of each impression were digitized with the following EOS:

- D810 (group D8I; Software Version Dental System 2014-1 × 64 - build 1.4.7.4-16.08.2018 Dental System, 3 Shape)
- In EOS X5 (group E5I; Software Version inLab SW 15.0, Dentsply Sirona)

Figure 3.3: Conventional impression with scannable PVS.

Afterward, cast models were procured after pouring the impressions with scannable Type IV plaster (Fino Scan Stone, LOT no 313096; FINO-Industrie Service GmbH, Brand-Erbisdorf, Germany). The impressions were separated from the casts after 60 minutes and the plaster models (Figure 3.4) were trimmed and stored for 24 hours in the same room under the same aforementioned ambient conditions. STL datasets of the plaster casts (n=25/group) were obtained through scanning with the same EOS as before.

Figure 3.4: Stone cast.

3.4 Analysis of Datasets

Analysis was conducted with Control 2015 after importing REF and test datasets. Artifacts were removed and margins were trimmed. In order to define a uniform spatial orientation of the datasets in the coordinate system, best fit alignment of the test datasets with REF was used in the area of the hemispheres located in the canine area, the second molar of the first quadrant, and the canine of the second quadrant (Figure 3.5).

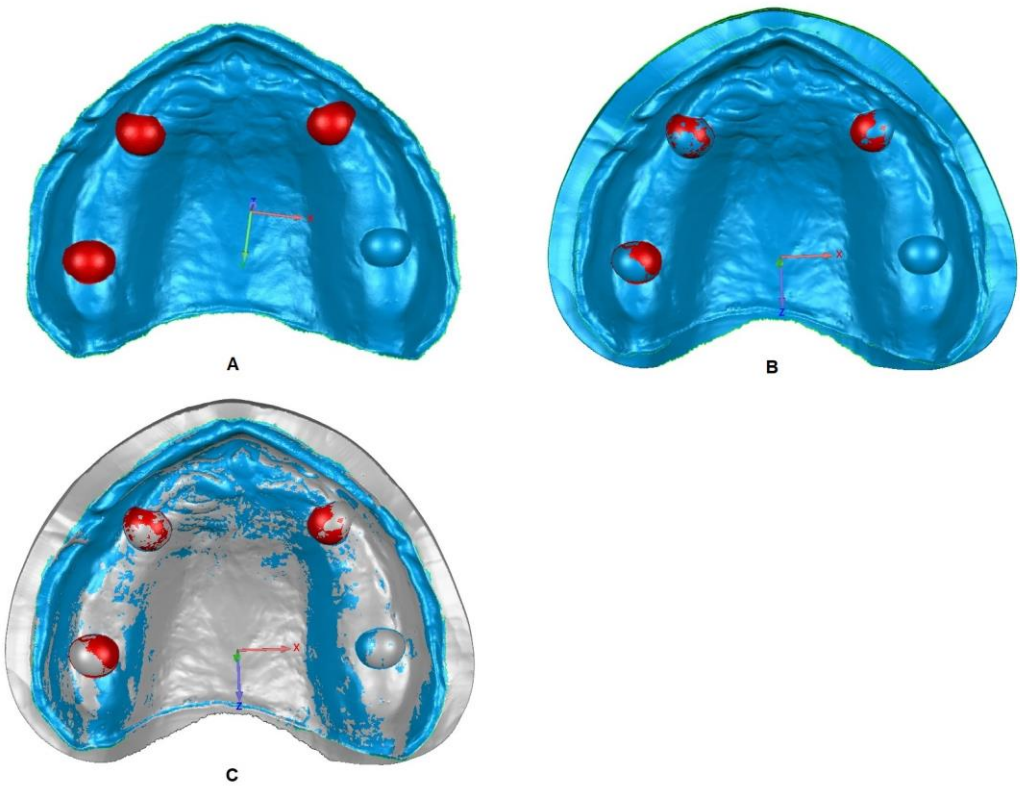

Figure 3.5: Test dataset orientation in the coordinate system. A Selection of spheres. B Best fit alignment over the selected area. C Test and REF datasets overlaid [119].

Following the alignment, the center of each hemisphere was identified using a system function, creating four virtual points named P17, P13, P23, and P27 (Figure 3.6). After that, the coordinates of points P17, P13, P23, and P27 and vectors P17-P13, P13-P23, P27-P23, and P17-P27 were introduced into Microsoft excel. Mathematical formulas were used to calculate the distances P17-P13, P17-P23, and P17-P27 (Figure 3.7) and angles between vector projections on the sagittal plane (YZ) and transverse plane (XZ).

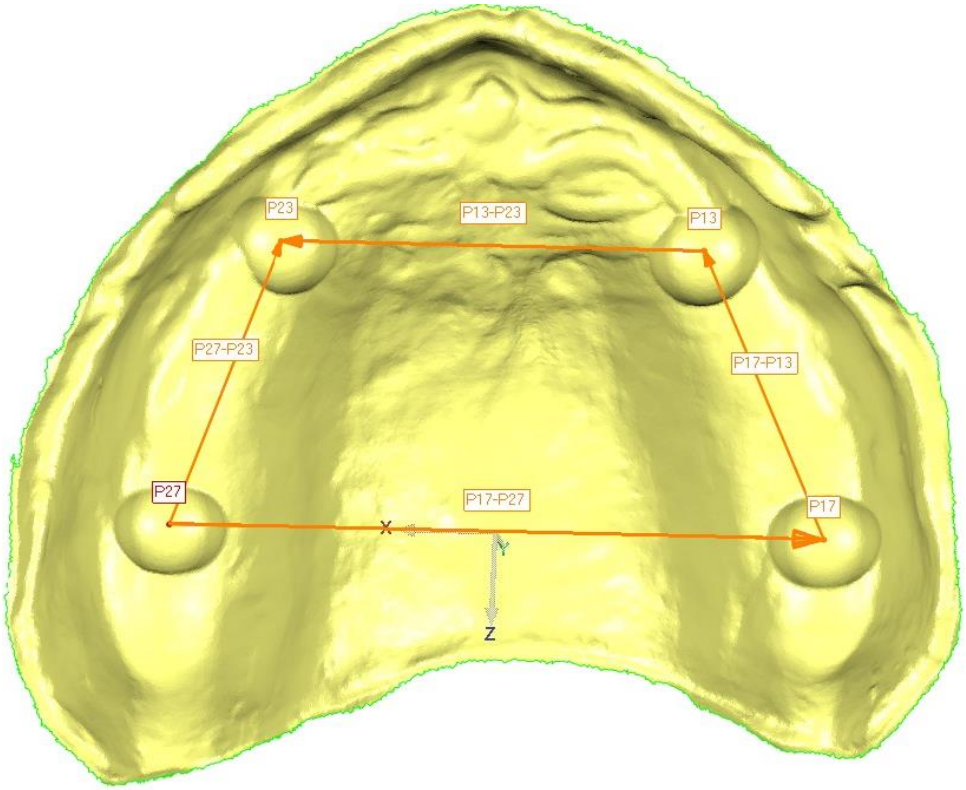

Figure 3.6: Points and vectors on the test dataset [119].

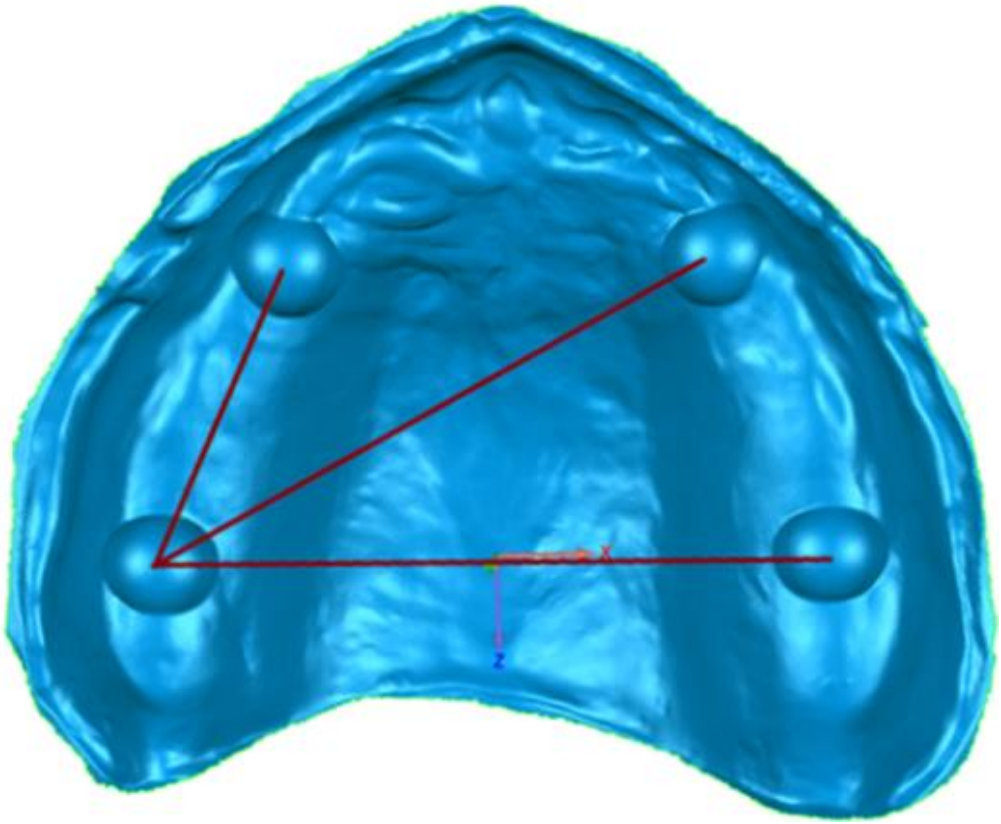

Figure 3.7: Distances P17-P13, P17-P23, and P17-P27 [119].

Length of P17-P13 = $\sqrt{(x(P13)-x(P17))^2+(y(P13)-y(P17))^2+(z(P13)-z(P17))^2}$

Length of P17-P23 = $\sqrt{(x(P23)-x(P17))^2+(y(P23)-y(P17))^2+(z(P23)-z(P17))^2}$

Length of P17-P27 = $\sqrt{(x(P27)-x(P17))^2+(y(P27)-y(P17))^2+(z(P27)-z(P17))^2}$

Angle $_{\text{transverse}} = arccos\frac{X(P17-P13)*X(P27-P23)+Z(P17-P13)*Z(P27-P23)}{\sqrt{X(P17-P13)^2+Z(P17-P13)^2}*\sqrt{X(P27-P23)^2+Z(P27-P23)^2}}*\frac{180}{\pi}$

Angle $_{\text{sagittal}} = arccos\frac{Y(P17-P13)*Y(P27-P23)+Z(P17-P13)*Z(P27-P23)}{\sqrt{Y(P17-P13)^2+Z(P17-P13)^2}*\sqrt{Y(P27-P23)^2+Z(P27-P23)^2}}*\frac{180}{\pi}$

where X, Y, and Z are the vector coordinates and x, y, and z are the coordinates of the points.

The differences for each measured parameter between the test datasets and the REF data were calculated.

3.5 Statistical Analysis

Statistical analysis was conducted with the Statistical Package for the Social Science, Version 25 (SPSS Inc., Chicago, USA). Descriptive statistics (mean, standard deviation, 95% confidence intervals) were given for each parameter and group. An analysis of variance (ANOVA) test was applied to assess the null hypothesis. Normality of data distribution was tested using Kolmogorov-Smirnov and Shapiro-Wilk test, followed by Levene's test to assess the obtained values for homogeneity. Significant differences between groups were evaluated by a post-hoc Games-Howell test. The level of significance was set at p=0.05.

4. Results

Table 4.1 reports the descriptive statistics, mean values, standard deviations (SD), and 95% confidence interval (CI) for each parameter. Table 4.2 and Table 4.3 depict the p values of the Games-Howell post-hoc test. Figure 4.1 and Figure 4.2 show the boxplots of linear and angular parameters respectively. The Kolmogorov Smirnov and Shapiro-Wilk tests revealed that 19 out of 45 groups were not normally distributed. The Levene's test based on mean values found no homogeneity for all tested parameters.

4.1 Trueness

4.1.1 Trueness of linear distances

4.1.1.1 Distance P17-P13

E5I (mean 4.58± 58.16), PRI (mean -5.52 ± 13.67), OMN (mean -6.52 ± 16.41) and D8I (mean -4.65 ± 10.40) showed the highest trueness ($p<0.001$). ITE (mean -51.26 ± 19.25) exhibited the significant highest negative aberration ($p<0.001$ to $p=0.002$), while TRS (mean 37.16 ± 35.55), TRD (mean 24.32 ± 12.62), E5M (mean 25.69 ± 24.51) and D8M (mean 35.77 ± 23.99) showed the significant highest positive aberration to REF ($p<0.001$).

4.1.1.2 Distance P17-P23

The best trueness was demonstrated by E5I (mean 2.39 ± 122.07) with PRI (mean -7.64 ± 23.44), D8I (mean -8.12 ± 9.45), TRS (mean 17.52 ± 44.20), OMN (mean 28.84 ± 79.15), E5M (mean 68.14 ± 32.92) and D8M (mean 81.83 ± 98.40) in the same value

range (p<0.001 to p=0.020). ITE (mean -91.59 ± 26.65) resulted in the significant highest negative aberration (p<0.001 to p=0.020), while TRD (mean 106.84 ± 32.76) produced significantly highest positive aberration to REF (p<0.001 to p=0.008).

4.1.1.3 Distance P17-P27

PRI (mean 3.39 ± 27.83) presented the best trueness with E5I (mean -10.74 ± 135.04), TRS (mean 18.87 ± 46.50) and D8I (mean -19.78 ± 13.59) in the same value range (p<0.001 to p=0.048). ITE (mean -109.94 ± 31.71) resulted in the significant highest negative aberration (p<0.001 to p=0.031), while TRD (mean 143.67 ± 49.40) displayed the significant highest positive aberration to REF (p<0.001).

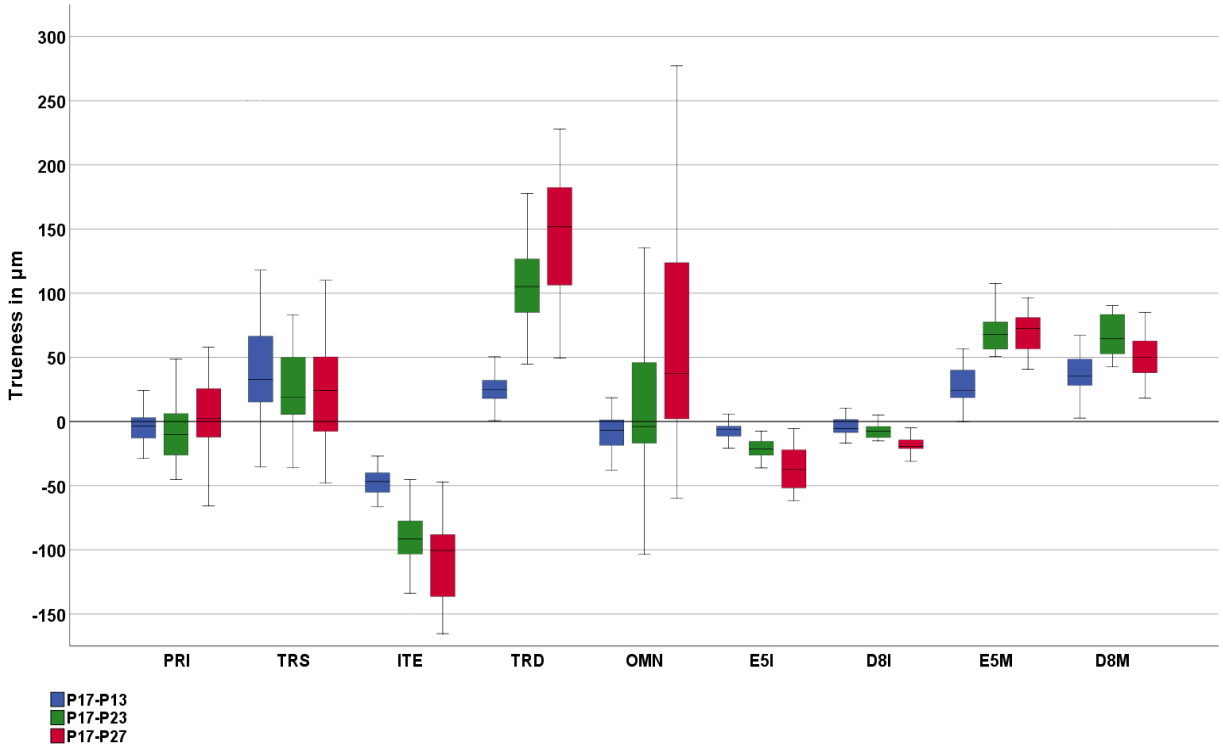

Figure 4.1: Boxplots for linear parameters.

4.1.2 Trueness of angles

4.1.2.1 Angle on the sagittal plane (angle YZ)

The lowest trueness was found for TRS (mean -0.11 ± 0.09), showing the highest negative aberration (p=0.001 to p=0.038) and for OMN (mean 0.19 ± 0.30) showing the highest positive aberration to REF (p=0.001 to p=0.008).

4.1.2.2 Angle on the transverse plane (angle XZ)

The lowest trueness was found for ITE (mean -0.15 ± 0.08) showing the highest negative aberration (p<0.001 to p=0.015) and for TRD (mean 0.11 ± 0.12) showing the highest positive aberration to REF (p<0.001 to p=0.001).

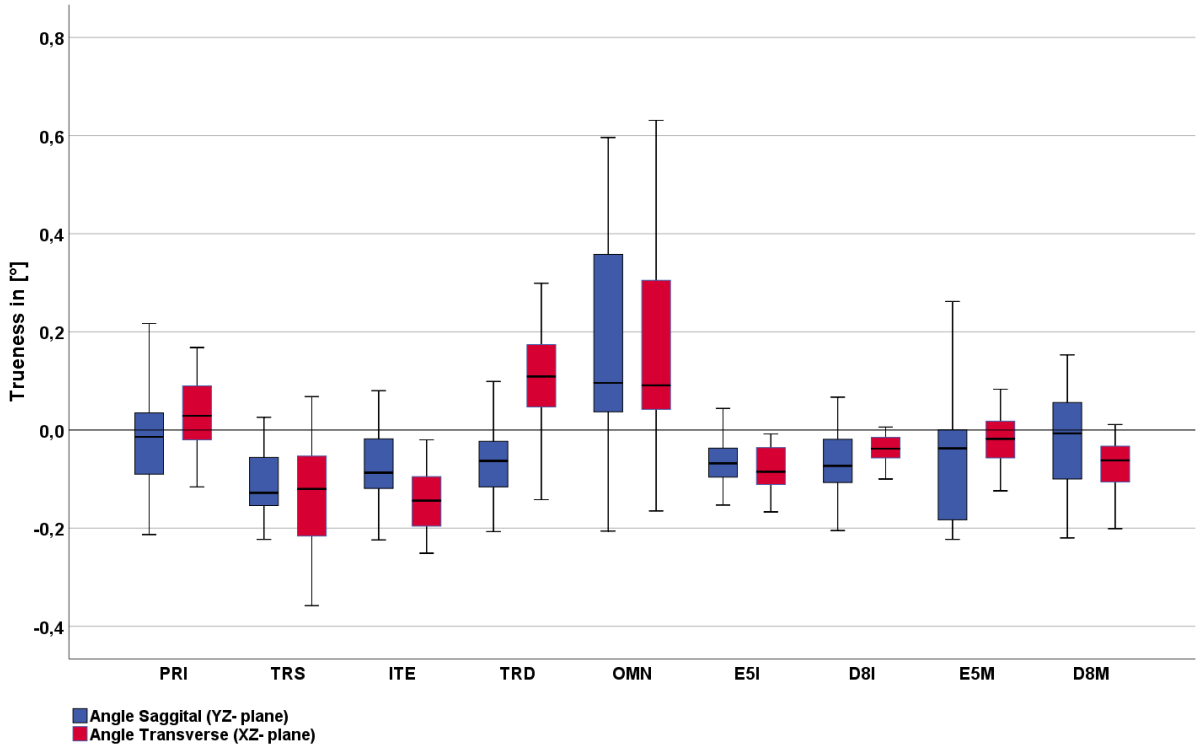

Figure 4.2: Boxplots for angular parameters.

4.2 Precision

For the determination of precision, the standard deviation of the groups in each parameter was adopted.

4.2.1 Precision of linear distances

4.2.1.1 Distance P17-P13

Groups D8I (mean -4.65 ± 10.40), TRD (mean 24.32 ± 12.62), PRI (mean -5.52 ± 13.67), OMN (mean -6.52 ± 16.41), ITE (mean -51.26 ± 19.25), D8M (mean 35.77 ± 23.99, E5M (mean 25.69 ± 24.51), TRS (mean 37.16 ± 35.55), E5I depicted precision in descending order.

4.2.1.2 Distance P17-P23

Group D8I (mean -8.12 ± 9.45) was the most precise followed by PRI (mean -7.64 ± 23.44), ITE (mean -91.59 ± 26.65), TRD (mean 106.84 ± 32.76), E5M (mean 68.14 ± 32.92), TRS (mean 17.52 ± 44.20), OMN (mean 28.84 ± 79.15), D8M (mean 81.83 ± 98.40) and E5I (mean 2.39 ± 122.07).

4.2.1.3 Distance P17-P27

The best precision was revealed by group D8I (mean -19.78 ± 13.59) followed by groups PRI (mean 3.39 ± 27.83) and ITE (mean -109.94 ± 31.71). Groups D8M (mean 46.93 ± 32.67), E5M (mean 66.82 ± 32.85), TRS (mean 18.87 ± 46.50), TRD (mean 143.67 ± 49.40), E5I (mean -10.74 ± 135.04) and OMN (mean 80.46 ± 146.27) presented precision in descending order.

4.2.2 Precision of angles

4.2.2.1 Angle on the sagittal plane (angle YZ)

Group E5I showed the highest precision followed by groups ITE (mean -0.07 ± 0.07) and TRD (mean -0.07 ± 0.07) which depicted the same value. Groups D8I (mean -0.06 ± 0.08), TRS (mean -0.11 ± 0.09), PRI (mean -0.01 ± 0.10), D8M (mean -0.01 ± 0.13), E5M (-0.03 ± 0.18) and OMN (mean 0.19 ± 0.30) were the least precise in descending order.

4.2.2.2 Angle on the transverse plane (angle XZ)

Group D8I (mean -0.05 ± 0.04) was the most precise followed by group E5I (mean -0.08 ± 0.05). Groups PRI (mean 0.03 ± 0.07), D8M (mean -0.08 ± 0.07) and E5M (mean -0.02 ± 0.07) revealed the same value for precision. ITE (mean -0.15 ± 0.08), TRD (mean 0.11 ± 0.12), TRS (mean -0.15 ± 0.15) and OMN (mean 0.19 ± 0.32) demonstrated lower precision in descending order.

Table 4.1 Descriptive statistics with mean values (Mean), standard deviation (SD), and 95% confidence interval (CI) for all tested parameters.

		Direct Digitization					*Indirect Digitization of Impression*		*Indirect Digitization of the Model*	
		PRI	**TRS**	**ITE**	**TRD**	**OMN**	**E5I**	**D8I**	**E5M**	**D8M**
Distance P17-P13 [µm]	Mean	-5.52 ^{B}	37.16 ^{C}	-51.26 ^{A}	24.32 ^{C}	-6.52 ^{B}	4.58 ^{B,C}	-4.65 ^{B}	25.69 ^{C}	35.77 ^{C}
	SD	13.67	35.55	19.25	12.62	16.41	58.16	10.40	24.51	23.99
	95% CI Min/Max	-11.17 /0.12	22.49 /51.84	-59.20 /-43.31	19.12 /29.53	-13.30 /0.25	-19.43 /28.59	-8.94 /-0.35	15.57 /35.81	25.86 /45.67
Distance P17-P23 [µm]	Mean	-7.64 ^{B}	17.52 ^{B,D}	-91.59 ^{A}	106.84 ^{E}	28.84 ^{B,C,D}	2.39 ^{B,C,D}	-8.12 ^{B}	68.14 ^{C}	81.83 ^{C,D,E}
	SD	23.44	44.20	26.65	32.76	79.15	122.07	9.45	32.92	98.40
	95% CI Min/Max	-17.32 /2.03	-0.72 /35.77	-102.60 /-80.59	93.31 /120.36	-3.83 /61.51	-48.00 /52.78	-12.02 /-4.22	54.55 /81.73	41.21 /122.45
Distance P17-P27 [µm]	Mean	3.39 ^{C}	18.87 ^{C,D}	-109.94 ^{A}	143.67 ^{F}	80.46 ^{C,D,E,F}	-10.74 ^{B,C,D,E}	-19.78 ^{B}	66.82 ^{E}	46.93 ^{D,E}
	SD	27.83	46.50	31.71	49.40	146.27	135.04	13.59	32.85	32.67
	95% CI Min/Max	-8.10 /14.88	-0.32 /38.07	-123.03 /-96.85	123.28 /164.06	20.08 /140.84	-66.48 /45.00	-25.39 /-14.17	53.26 /80.38	33.44 /60.41
Angle sagittal YZ- plane [°]	Mean	-0.01 ^{B,C}	-0.11 ^{A}	-0.07 ^{A,B}	-0.07 ^{A,B}	0.19 ^{C}	-0.07 ^{A,B}	-0.06 ^{A,B}	-0.03 ^{A,B,C}	-0.01 ^{A,B,C}
	SD	0.10	0.09	0.07	0.07	0.30	0.06	0.08	0.18	0.13
	95% CI Min/Max	-0.06 /0.03	-0.14 /-0.07	-0.10 /-0.04	-0.10 /-0.04	0.07 /0.32	-0.09 /-0.04	-0.09 /-0.03	-0.11 /0.04	-0.07 /0.04
Angle transverse XZ-plane [°]	Mean	0.03 ^{E,F}	-0.15 ^{A,B}	-0.15 ^{A}	0.11 ^{F}	0.19 ^{E,F}	-0.08 ^{B,C}	-0.05 ^{C,D}	-0.02 ^{D,E}	-0.08 ^{A,B,C}
	SD	0.07	0.15	0.08	0.12	0.32	0.05	0.04	0.07	0.07
	95% CI Min/Max	0.00 /0.06	-0.21 /-0.09	-0.18 /-0.11	0.06 /0.16	0.06 /0.32	-0.10 /-0.06	-0.06/ -0.03	-0.05 /0.01	-0.11 /-0.05

A-F: Superscript letters indicate significant differences between digitization systems for single parameters.

Table 4.2 P-values of Games-Howell post-hoc analysis to detect significant differences in view of linear parameters. Bolded values denote significant differences.

		Direct Digitization					*Indirect Digitization of the Impression*		*Indirect Digitization of the Model*	
		PRI	**TRS**	**ITE**	**TRD**	**OMN**	**E5I**	**D8I**	**E5M**	**D8M**
PRI	P17-P13		**p<0.001**	**p<0.001**	**p<0.001**	p=1.000	p=0.994	p=1.000	**p<0.001**	**p<0.001**
	P17-P23		p=0.258	**p<0.001**	**p<0.001**	p=0.426	p=1.000	p=1.000	**p<0.001**	**p=0.004**
	P17-P27		p=0.880	**p<0.001**	**p<0.001**	p=0.239	p=1.000	**p=0.017**	**p<0.001**	**p<0.001**
TRS	P17-P13	**p<0.001**		**p<0.001**	p=0.741	**p<0.001**	p=0.317	**p<0.001**	p=0.917	p=1.000
	P17-P23	p=0.258		**p<0.001**	**p<0.001**	p=0.999	p=1.000	p=0.152	**p=0.001**	p=0.106
	P17-P27	p=0.880		**p<0.001**	**p<0.001**	p=0.551	p=0.979	**p=0.011**	**p=0.004**	p=0.276
ITE	P17-P13	**p<0.001**	**p<0.001**		**p<0.001**	**p<0.001**	**p=0.002**	**p<0.001**	**p<0.001**	**p<0.001**
	P17-P23	**p<0.001**	**p<0.001**		**p<0.001**	**p<0.001**	**p=0.020**	**p<0.001**	**p<0.001**	**p<0.001**
	P17-P27	**p<0.001**	**p<0.001**		**p<0.001**	**p<0.001**	**p=0.031**	**p<0.001**	**p<0.001**	**p<0.001**
TRD	P17-P13	**p<0.001**	p=0.741	**p<0.001**		**p<0.001**	p=0.765	**p<0.001**	p=1.000	p=0.482
	P17-P23	**p<0.001**	**p<0.001**	**p<0.001**		**p=0.002**	**p<0.001**	**p<0.001**	**p=0.004**	p=0.949
	P17-P27	**p<0.001**	**p<0.001**	**p<0.001**		p=0.525	**p<0.001**	**p<0.001**	**p<0.001**	**p<0.001**
OMN	P17-P13	p=1.000	**p<0.001**	**p<0.001**	**p<0.001**		p=0.990	p=1.000	**p<0.001**	**p<0.001**
	P17-P23	p=0.426	p=0.999	**p<0.001**	**p=0.002**		p=0.991	p=0.369	p=0.376	p=0.487
	P17-P27	p=0.239	p=0.551	**p<0.001**	p=0.525		p=0.368	p=0.048	p=1.000	p=0.966
E5I	P17-P13	p=0.994	p=0.317	**p=0.002**	p=0.765	p=0.990		p=0.996	p=0.758	p=0.280
	P17-P23	p=1.000	p=1.000	**p=0.020**	**p=0.008**	p=0.991		p=1.000	p=0.232	p=0.244
	P17-P27	p=1.000	p=0.979	**p=0.031**	**p<0.001**	p=0.368		p=1.000	p=0.165	p=0.509
D8I	P17-P13	p=1.000	**p<0.001**	**p<0.001**	**p<0.001**	p=1.000	p=0.996		**p<0.001**	**p<0.001**
	P17-P23	p=1.000	p=0.152	**p<0.001**	**p<0.001**	p=0.369	p=1.000		**p<0.001**	**p=0.003**
	P17-P27	**p=0.017**	**p=0.011**	**p<0.001**	**p<0.001**	**p=0.048**	p=1.000		**p<0.001**	**p<0.001**
E5M	P17-P13	**p<0.001**	p=0.917	**p<0.001**	p=1.000	**p<0.001**	p=0.758	**p<0.001**		p=0.864
	P17-P23	**p<0.001**	**p=0.001**	**p<0.001**	**p=0.010**	p=0.370	p=0.232	**p<0.001**		p=0.298
	P17-P27	**p<0.001**	**p=0.004**	**p<0.001**	**p<0.001**	p=1.000	p=0.165	**p<0.001**		p=0.455
D8M	P17-P13	**p<0.001**	p=1.000	**p<0.001**	p=0.482	**p<0.001**	p=0.280	**p<0.001**	p=0.864	
	P17-P23	**p=0.004**	p=0.106	**p<0.001**	p=0.949	p=0.487	p=0.244	**p=0.003**	p=0.999	
	P17-P27	**p<0.001**	p=0.276	**p<0.001**	**p<0.001**	p=0.966	p=0.509	**p<0.001**	p=0.455	

Table 4.3 P-values of Games-Howell post-hoc analysis to detect significant differences in view of angular parameters. Bolded values denote significant differences.

		Direct Digitization					*Indirect Digitization of the Impression*		*Indirect Digitization of the Model*	
		PRI	**TRS**	**ITE**	**TRD**	**OMN**	**E5I**	**D8I**	**E5M**	**D8M**
PRI	YZ		**p=0.038**	p=0.322	p=0.453	p=0.055	p=0.386	p=0.666	p=1.000	p=1.000
	XZ		**p=0.001**	**p<0.001**	p=0.148	p=0.309	**p<0.001**	**p=0.001**	p=0.273	**p<0.001**
TRS	YZ	**p=0.038**		p=0.896	p=0.813	**p=0.001**	p=0.734	p=0.666	p=0.701	p=0.112
	XZ	**p=0.000**		p=1.000	**p<0.001**	**p=0.001**	p=0.363	**p=0.039**	**p=0.007**	p=0.450
ITE	YZ	p=0.322	p=0.896		p=1.000	**p=0.005**	p=1.000	p=1.000	p=0.981	p=0.523
	XZ	**p<0.001**	p=1.000		**p<0.001**	**p=0.001**	**p=0.015**	**p<0.001**	**p<0.001**	p=0.056
TRD	YZ	p=0.453	p=0.813	p=1.000		**p=0.006**	p=1.000	p=1.000	p=0.992	p=0.639
	XZ	p=0.148	**p<0.001**	**p<0.001**		p=0.951	**p<0.001**	**p<0.001**	**p=0.001**	**p<0.001**
OMN	YZ	p=0.055	**p=0.001**	**p=0.005**	**p=0.006**		**p=0.005**	**p=0.008**	p=0.053	p=0.073
	XZ	p=0.309	**p=0.001**	**p=0.001**	p=0.951		**p=0.008**	**p=0.028**	p=0.076	**p=0.008**
E5I	YZ	p=0.386	p=0.734	p=1.000	p=1.000	**p=0.005**		p=1.000	p=0.991	p=0.599
	XZ	**p<0.001**	p=0.363	**p=0.015**	**p<0.001**	**p=0.008**		p=0.151	**p=0.018**	p=1.000
D8I	YZ	p=0.666	p=0.666	p=1.000	p=1.000	**p=0.008**	p=1.000		p=0.998	p=0.796
	XZ	**p=0.001**	p=0.039	**p<0.001**	**p<0.001**	**p=0.028**	p=0.151		p=0.745	p=0.384
E5M	YZ	p=1.000	p=0.701	p=0.981	p=0.992	p=0.053	p=0.991	p=0.998		p=1.000
	XZ	p=0.273	**p=0.007**	**p<0.001**	**p=0.001**	p=0.076	**p=0.018**	p=0.745		**p=0.049**
D8M	YZ	p=1.000	p=0.112	p=0.523	p=0.639	p=0.073	p=0.599	p=0.796	p=1.000	
	XZ	**p<0.001**	p=0.450	p=0.056	**p<0.001**	**p=0.008**	p=1.000	p=0.384	**p=0.049**	

5. Discussion

Different direct and indirect digitization methods of edentulous jaws were compared with regards to accuracy (trueness and precision) in view of linear and angular deviations in the resulting model data. Significant differences were revealed for trueness between most of the digitization systems in every measured aspect. Accordingly, the null hypothesis had to be rejected.

5.1 Discussion of Results

The current results can be compared to prior investigations with similar methodology (calculation of linear distortions between implants or implant-like objects). In an analogous setting, the measurement of linear distances between spheres on an edentulous maxilla revealed similar trueness across the arch for Trios 3 and iTero, while iTero exhibited significantly more negative values within a quadrant, akin to our current results despite the use of a different scanning protocol [120]. Brian et al. reported larger errors for Cerec AC Omnicam and Trios 3 and lower errors for iTero in digitizing an edentulous mandible with cylindrical structures [121]. Ciocca et al. measured similar inaccuracies in the diagonal (0.058mm to 0.158mm), larger within one quadrant (0.054mm to 0.100mm) and lower across the arch (-0.121mm to 0.121mm) using True Definition [122]. In a previous examination, no statistical differences were found between iTero, Trios 3, and True Definition within a quadrant and diagonally, however additional landmarks were used to enhance the scanning procedure [96]. Mandelli et al. described significantly better linear accuracies between implants on an edentulous maxilla with the True Definition Scanner, which might be

attributed to different scanning strategies employed [123]. Mangano et al. evaluated the linear error of Trios 3, iTero, Cerec Omnicam, and Cerec Primescan between scan bodies on an edentulous maxillary model and reported no statistical differences between iTero, Primescan, and Omnicam but higher overall error for Trios 3 [124]. In a comparison of scan body distances on an edentulous mandible, lower trueness was reported for True Definition Scanner to stone casts generated after vinyl polysiloxane impressions [125].

Researchers have frequently pointed out a correlation between horizontal error increase with growing measured spans on the edentulous arch [72, 126-128]. This phenomenon appears to be related to the progressive accumulation of inaccuracies during the matching of captured images. Captured images have to be stitched together, causing distortions to combine and increase the overall error of the generated dataset [72, 98, 129]. Currently, most tested IOS revealed a similar pattern (Figure 5.1). By contrast, digitization with EOS (in the present study: D810 and In Eos X5) does not exhibit an analogous distortion pattern (Figure 5.2). EOS are more efficient in capturing larger segments of the model or the impression at the same time, therefore fewer images are necessary and can be more precisely matched together. Consequently, the error caused by image superimposition seems to be less pronounced with EOS [128]. Moreover, indirect digitization is conducted under regulated conditions, with a highly automated process, and offers exceptional reproducibility [130]. Currently, impression digitization with D810 demonstrated the highest precision. However, with the digitization of impressions and casts, errors generated with the conventional methods usually related to gypsum expansion or impression material shrinkage and deformation are integrated to the resulting dataset.

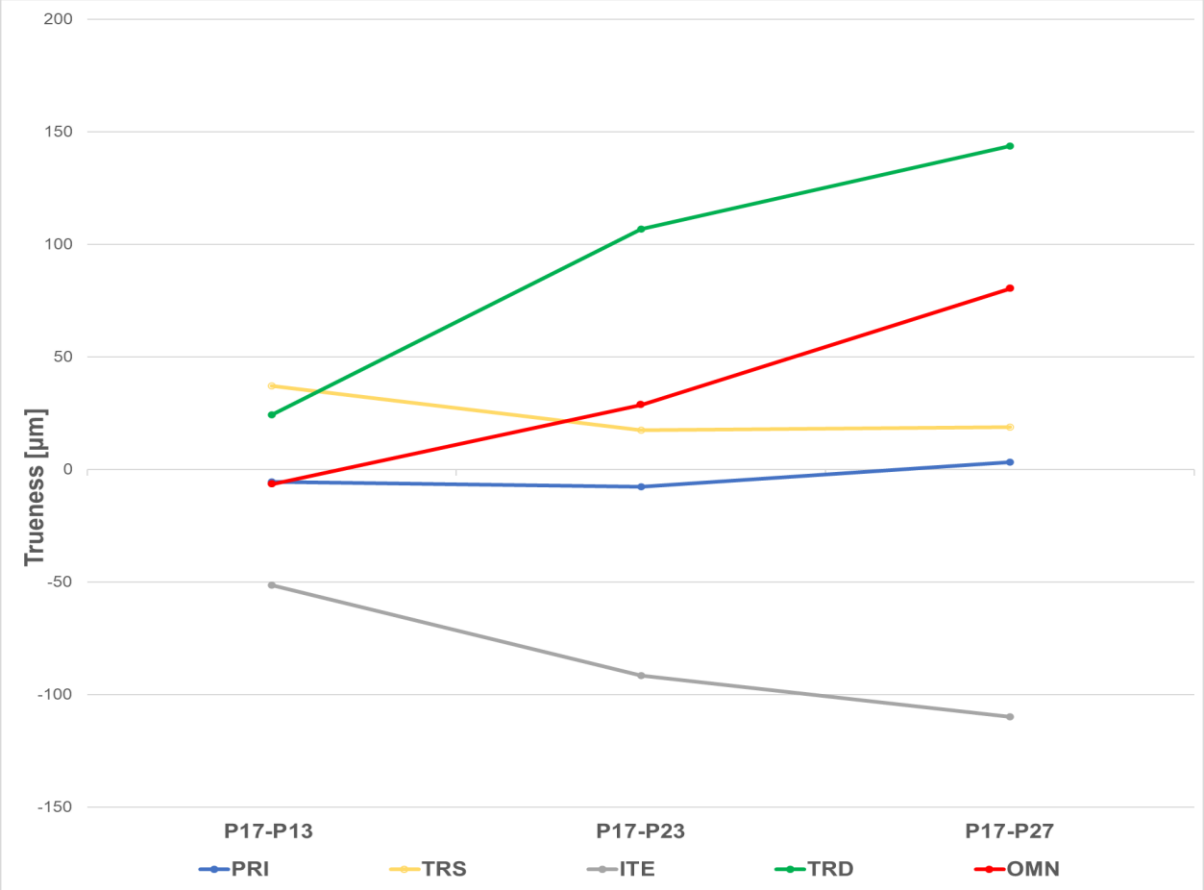

Figure 5.1 Trueness of IOS (linear parameters).

Furthermore, the accuracy of indirect digitization has been proven to be dependent on the surface reflectivity and geometry of the scanned object, as highly reflective materials and areas with narrow and deep hollow spaces and inside contours present challenges for laboratory scanners [131, 132]. For fully dentate arches, the digitization of stone models was stated to be more accurate than the direct digitization of impressions [11]. Presently, digitized impressions revealed similar or even superior trueness to digitized stone casts. This difference could be attributed to the scannable impression material and the geometry of the testing model. Edentulous arches present relatively simpler forms with scarcely any undercuts, which can be recorded by optical scanners more effectively, while distortions resulting during impression setting and removal are less pronounced [133, 134].

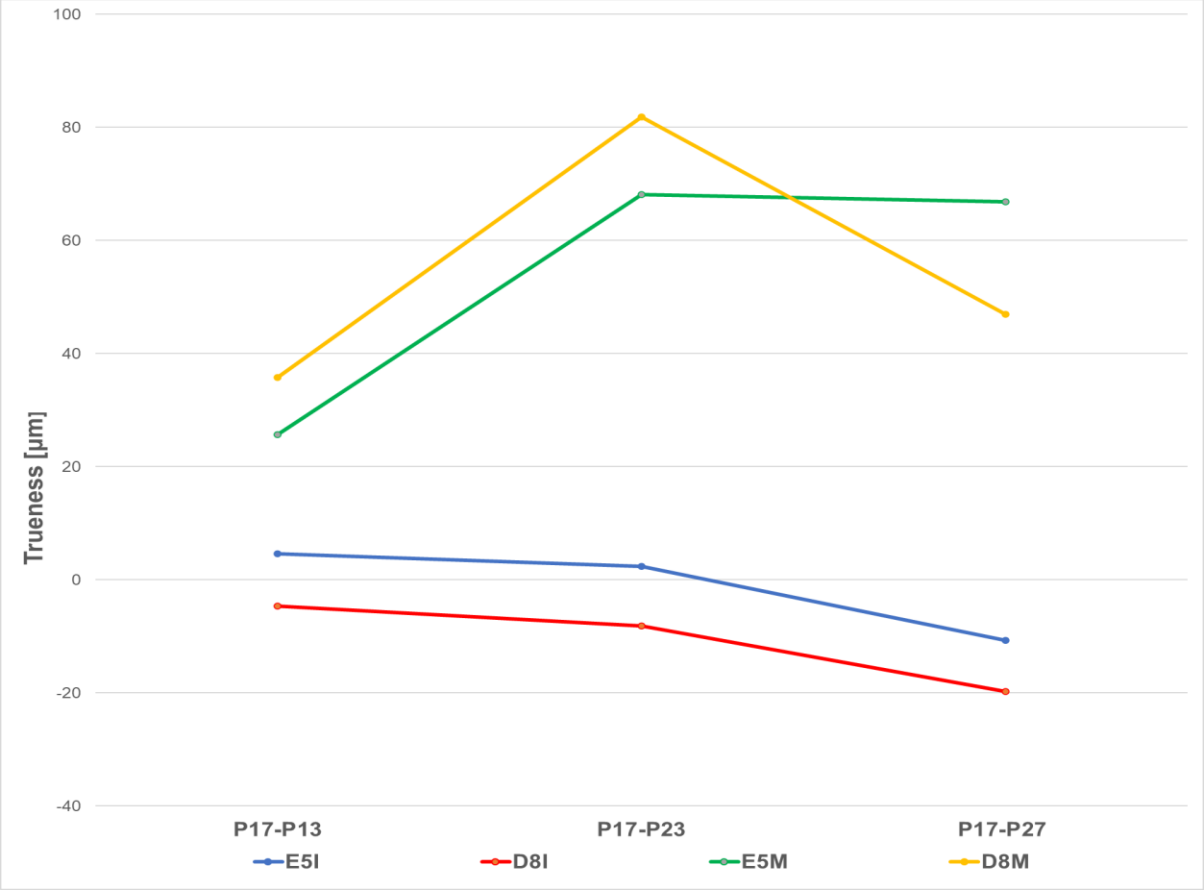

Figure 5.2 Trueness of EOS (linear parameters).

Moreover, impression digitization demonstrated similar results to Cerec Primescan and Cerec AC Omnicam, similar to the findings of Chebib et. al with Trios 3 and digitized PVS impressions on an edentulous maxilla [135]. Stone cast digitization revealed comparable trueness to Cerec AC Omnicam, Trios 3, and True Definition in accordance with recent findings [107], but was less accurate than Cerec Primescan AC.

Regarding angular differences, in examinations with similar methodology, lower vertical angle deviations were measured for Trios 3 and True Definition compared to Cerec AC Omnicam on a fully dentate model [69]. A prior investigation revealed no angular discrepancies between direct digitization with iTero and indirect digitization of impressions and stone casts on a fully dentate model [11]. Contrary to current results, two recent publications reported higher angular discrepancies for Trios 3 compared to

conventional impressions [136, 137] and to iTero [137] on edentulous models in vitro. Schmidt et al. reported significantly higher vertical torsion with True Definition than Cerec Omnicam and Trios 3 on a fully dentate model [116].

Each method generates a different distortion pattern, which can be further examined through analysis of the linear parameters in combination with angle measurements. True definition and Cerec Primescan AC exhibited an increased angle in the XZ plane along with larger P17-P27 distance, reflecting a transverse expansion of the posterior part of the edentulous arch. On the other hand, Trios 3 and stone cast digitization presented a smaller XZ angle and increased P17-P27 distance reflecting an increased linear shift between the two hemi arches along the Z-axis in the horizontal plane. The larger values of the XZ and XY angles presented by Cerec AC Omnicam can be explained as expansion in both the sagittal and traverse dimensions. In the case of iTero and impression digitization, a posterior contraction occurs primarily in the transverse plane. Analogous patterns were previously reported for Cerec Omnicam [92], iTero [95, 138], and Trios 3 [95]. Differences in the resulting distortion presented by each IOS can be attributed to the varying optical technologies and individual software algorithms employed by each system [110]. Regarding indirect digitization with EOS, digitization of stone casts exhibited positive error in all measured distances as well as in angle XZ corresponding to the gypsum expansion (0.06% according to the manufacturer) [139]. At the same time, the negative errors registered in most distances for impression digitization can be explained by the shrinkage of the PVS impression material of 0.04% [140].

5.2 Discussion of Materials and Methods

Presently, linear and angular discrepancies were measured between four hemispheres on an edentulous maxillary model. Most commonly, the accuracy of digital models can be assessed either through the calculation of differences between surface points after dataset superimposition or the metrical comparison of reference geometries [11]. Although dataset superimposition with best-fit algorithms seems to be the method of choice for most researchers, its limitations have been widely discussed [13, 91, 92, 129, 135, 141]. Criticism over error underestimation due to the dataset orientation in a position of least aberration and the errors caused by the iterative algorithm has been voiced by several authors [69, 115, 127, 130]. O'Toole et al. proved that best fit alignment results in the closer arrangement of point clouds and consequently greater miscalculation, as errors are spread evenly across the dataset [114]. Güth et al. postulated this error to be acceptable for calculations up to one quadrant but detrimental to comparisons of larger datasets, including complete arches [115]. Nonetheless, in vivo acquisition of a highly accurate dataset of the clinical situation, which is required for comparisons on the basis of reference geometries, is challenging, particularly for edentulous jaws. Moreover, spherical reference geometries have been frequently used for the investigation of accuracy on fully dentate arches [69, 116, 130].

The present study, although relevant with regard to future clinical applications and scientific progress, is still affected by certain limitations. Firstly, the accuracy of digitization was evaluated only for the upper jaw, which has a large palatal area that may allow for more precise matching of captured images. This peculiarity has been discussed to increase the overall accuracy of the scanning procedure [69]. By contrast,

the lower jaw’s smaller areas of attached mucosa and the absence of anatomic landmarks, which render scanning procedures more demanding [98, 101].

The current investigation was carried out by the same skilled professional, in a laboratory setting, in accordance with clinical specifications. However, results could vary significantly in vivo, as the influence of patient's movement, saliva and restricted maneuverability in the oral cavity cannot be adequately reproduced extraorally. In addition, it should be noted that the use of a PEEK testing model, with different optical properties than the intraoral mucosa, might have improved the scanning efficiency and accuracy of the IOS [72]. Furthermore, the model was recorded using a scan path which has yet to be validated for completely edentulous situations.

5.3 Clinical Considerations

Given that the tolerance for complete denture fabrication is defined by the mucosal resilience, which has been reported to be in a range of 300 to 500μm [93, 108], all investigated methods produced clinically acceptable results. The majority of previous research concurred that IOS can produce impressions with an accuracy below the threshold for complete denture fabrication [106-108]. However, IOS achieve a pressureless, mucostatic record of the edentulous anatomy, without extension of the mobile mucosa under muscle movement or compression of the highly resilient posterior palatal areas [135]. Generally, functional impression of the border and the subsequent marginal and palatal seal of the denture are up to now unattainable with direct digitization [55, 94]. Although, thus far scientific research has not confirmed the merit of a peripheral and palatal seal [142]. Moreover, denture retention can be achieved according to the mucostatic principle, through surface tension between the intaglio surface of the denture and the underlying mucosa, independent of palatal

marginal seal and functional valves [24]. As CAM manufactured dentures demonstrate a superior fit and thusly more intimate contact to the underlying mucosa compared to conventionally manufactured ones, the mucostatic principle might contribute more to denture retention [57-61]. Consequently, the shortcomings of intraoral scans of edentulous arches could be mitigated to a certain extent by their superior accuracy, which translates to better congruence between the denture base and the underlying tissues. Nevertheless, a completely digital workflow for the construction of CAD/CAM dentures has not been proven to reliably produce clinically sufficient retention [54, 101, 102]. Currently Cerec Primescan AC demonstrated trueness values similar to impression digitization and superior to stone cast digitization for most parameters, while Trios 3 and Cerec AC Omnicam performed similarly to stone cast digitization, suggesting that a highly accurate dataset and the resulting precise fit may be possible with intraoral digitization. On the other hand, the digitization of functional impressions and cast models ensures the existence of a peripheral seal without relining [135] and has been shown to produce more accurate results [54].

Nevertheless, IOS could be useful for the acquisition of preliminary impressions, digital prosthetic planning, implant planning, or in situations where conventional impressions are challenging such as patients with strong gag reflex [143] or restricted mouth opening [144, 145]. Furthermore, immediate dentures could be manufactured using data recorded through direct digitization, since the peripheral and palatal seal can be secondarily achieved through the eventual reline of the base [54]. In addition, a pressureless mucostatic impression procured with IOS may be favorable for patients with mobile tissues [24, 93].

6. Conclusions

Given the current study's limitations, it could be concluded that:

- In view of linear parameters, direct digitization with Cerec Primescan AC and indirect digitization of conventional impression presented the highest trueness, while impression digitization with the D810 laboratory scanner revealed the highest precision.
- Concerning angular parameters digitization of stone cast models resulted in significantly higher trueness than any other method. Digitization of impressions showed considerably better precision.
- Cerec Primescan AC demonstrated trueness similar to impression digitization and superior to stone cast digitization. Trios 3 and Cerec AC Omnicam performed similarly to indirect digitization of impressions and stone casts.
- Given the tolerance for complete denture fabrication all investigated methods seem to exhibit accuracies within clinically acceptable levels.

7. References

1. Tyrovolas, S., et al., *Population prevalence of edentulism and its association with depression and self-rated health.* Scientific Reports, 2016. **6**(1): p. 37083.
2. Jordan, R.A., et al., *The Fifth German Oral Health Study (Fünfte Deutsche Mundgesundheitsstudie, DMS V) - rationale, design, and methods.* BMC Oral Health, 2014. **14**: p. 161.
3. Carlsson, G. and R. Omar, *The future of complete dentures in oral rehabilitation. A critical review.* J Oral Rehabil, 2010. **137**: p. 146-156.
4. Schweiger, J., et al., *Virtual evaluation for CAD-CAM-fabricated complete dentures.* J Prosthet Dent, 2017. **117**(1): p. 28-33.
5. Alghazawy, T., *Advancements in CAD/CAM technology: Options for practical implementation.* Journal of Prosthodontic Research, 2016. **60**.
6. Schweiger, J., et al., *Systematics and concepts for the digital production of complete dentures: risks and opportunities.* Int J Comput Dent, 2018. **21**(1): p. 41-56.
7. Janeva, N., et al., *Advantages of CAD/CAM versus Conventional Complete Dentures - A Review.* Open Access Macedonian Journal of Medical Sciences, 2018. **6**.
8. Baba, N.Z., et al., *CAD/CAM Complete Denture Systems and Physical Properties: A Review of the Literature.* J Prosthodont, 2021. **30**(S2): p. 113-124.
9. Zimmermann, M., et al., *Intraoral scanning systems - a current overview.* Int J Comput Dent, 2015. **18**(2): p. 101-29.
10. Mangano, F., et al., *Intraoral scanners in dentistry: a review of the current literature.* BMC Oral Health, 2017. **17**(1): p. 149.
11. Keul, C. and J.F. Güth, *Accuracy of full-arch digital impressions: an in vitro and in vivo comparison.* Clin Oral Investig, 2020. **24**(2): p. 735-745.
12. Keul, C., et al., *Fit of 4-unit FDPs made of zirconia and CoCr-alloy after chairside and labside digitalization--a laboratory study.* Dent Mater, 2014. **30**(4): p. 400-7.
13. Ender, A., T. Attin, and A. Mehl, *In vivo precision of conventional and digital methods of obtaining complete-arch dental impressions.* J Prosthet Dent, 2016. **115**(3): p. 313-20.
14. Kravitz, N., et al., *Intraoral digital scanners.* Journal of clinical orthodontics : JCO, 2014. **48**: p. 337-347.
15. Khalifa, N., *Digital Impressions*, in *Digitization in Dentistry: Clinical Applications*, P. Jain and M. Gupta, Editors. 2021, Springer International Publishing: Cham. p. 169-187.
16. Mohamad Rasidi, M.Q.Z.B., *Review on History of Complete Denture.* Research Journal of Pharmacy and Technology, 2016. **9**: p. 1069.
17. Krsek, H. and N. Dulcic, *Functional Impressions in Complete Denture and Overdenture Treatment.* Acta Stomatol Croat, 2015. **49**(1): p. 45-53.
18. Petrie, C.S., M.P. Walker, and K. Williams, *A survey of U.S. prosthodontists and dental schools on the current materials and methods for final impressions for complete denture prosthodontics.* J Prosthodont, 2005. **14**(4): p. 253-62.
19. Basker, R.M., J.C. Davenport, and H.R. Tomlin, *Prosthetic Treatment of the Edentulous Patient.* 2017.

20. *Principles, concepts, and practices in prosthodontics--1994. Academy of Prosthodontics.* J Prosthet Dent, 1995. **73**(1): p. 73-94.
21. Jacobson, T.E. and A.J. Krol, *A contemporary review of the factors involved in complete denture retention, stability, and support. Part I: retention.* J Prosthet Dent, 1983. **49**(1): p. 5-15.
22. Jacobson, T.E. and A.J. Krol, *A contemporary review of the factors involved in complete dentures. Part II: stability.* J Prosthet Dent, 1983. **49**(2): p. 165-72.
23. Jacobson, T.E. and A.J. Krol, *A contemporary review of the factors involved in complete dentures. Part III: support.* J Prosthet Dent, 1983. **49**(3): p. 306-13.
24. Bohannan, H.M., *A critical analysis of the mucostatic principle.* The Journal of Prosthetic Dentistry, 1954. **4**(2): p. 232-241.
25. *Textbook of removable prosthodontics : the Scandinavian approach*. 2020.
26. Zarb, G.A. and C.L. Bolender, *Prosthodontic treatment for edentulous patients*. 2004, St. Louis: Mosby.
27. Wicks, R., S. Ahuja, and V. Jain, *Defining the posterior palatal seal on a definitive impression for a maxillary complete denture by using a nonfluid wax addition technique.* J Prosthet Dent, 2014. **112**(6): p. 1597-600.
28. Binti, N., M. Sunil, and A. Jain, *Knowledge, Attitude and Perception of Materials and Methods Used for Recording Posterior Palatal Seal Among Dental Practitioners and Dental Students.* Biomedical and Pharmacology Journal, 2018. **11**: p. 539-551.
29. Daou, E.E., *The elastomers for complete denture impression: A review of the literature.* Saudi Dent J, 2010. **22**(4): p. 153-60.
30. Genieser, A. and H. Jakstat, *[Methods and materials for the construction of complete dentures].* Dtsch Zahnarztl Z, 1990. **45**(9): p. 559-60.
31. Rubel, B., *Impression Materials: A Comparative Review of Impression Materials Most Commonly Used in Restorative Dentistry.* Dental clinics of North America, 2007. **51**: p. 629-42, vi.
32. *PHILLIPS' SCIENCE OF DENTAL MATERIALS*. 2021, [S.l.]: SAUNDERS.
33. Islamova, R., et al., *bis-Nitrile and bis-Dialkylcyanamide Platinum(II) Complexes as Efficient Catalysts for Hydrosilylation Cross-Linking of Siloxane Polymers.* Molecules, 2016. **21**: p. 311.
34. Naumovski, B. and B. Kapushevska, *Dimensional Stability and Acuracy of Silicone - Based Impression Materials Using Different Impression Techniques - A Literature Review.* Pril (Makedon Akad Nauk Umet Odd Med Nauki), 2017. **38**(2): p. 131-138.
35. Donovan, T.E. and W.W. Chee, *A review of contemporary impression materials and techniques.* Dent Clin North Am, 2004. **48**(2): p. vi-vii, 445-70.
36. Hamalian, T.A., E. Nasr, and J.J. Chidiac, *Impression materials in fixed prosthodontics: influence of choice on clinical procedure.* J Prosthodont, 2011. **20**(2): p. 153-60.
37. Vitti, R.P., et al., *Dimensional accuracy of stone casts made from silicone-based impression materials and three impression techniques.* Braz Dent J, 2013. **24**(5): p. 498-502.
38. Faria, A.C., et al., *Accuracy of stone casts obtained by different impression materials.* Braz Oral Res, 2008. **22**(4): p. 293-8.
39. Massad, J. and D. Cagna, *Vinyl polysiloxane impression material in removable prosthodontics. Part 1: edentulous impressions.* Compendium of continuing education in dentistry, 2007. **28 8**: p. 452-9; quiz 460, 470.

40. Zarone, F., et al., *Accuracy of Three Impression Materials on the Totally Edentulous Maxilla: In Vitro/In Silico Comparative Analysis.* Materials (Basel), 2020. **13**(3).
41. Johnson, G., X. Lepe, and T. Aw, *The effect of surface moisture on detail reproduction of elastomeric impressions.* The Journal of prosthetic dentistry, 2003. **90**: p. 354-64.
42. Walker, M.P., et al., *Moisture effect on polyether and polyvinylsiloxane dimensional accuracy and detail reproduction.* J Prosthodont, 2005. **14**(3): p. 158-63.
43. Pandey, P., et al., *Mechanical Properties of a New Vinyl Polyether Silicone in Comparison to Vinyl Polysiloxane and Polyether Elastomeric Impression Materials.* Contemp Clin Dent, 2019. **10**(2): p. 203-207.
44. Maeda, Y., et al., *A CAD/CAM system for removable denture. Part I: Fabrication of complete dentures.* Int J Prosthodont, 1994. **7**(1): p. 17-21.
45. Kawahata, N., et al., *Trial of duplication procedure for complete dentures by CAD/CAM.* J Oral Rehabil, 1997. **24**(7): p. 540-8.
46. Sun, Y., P. Lü, and Y. Wang, *Study on CAD&RP for removable complete denture.* Comput Methods Programs Biomed, 2009. **93**(3): p. 266-72.
47. Busch, M. and B. Kordass, *Concept and development of a computerized positioning of prosthetic teeth for complete dentures.* Int J Comput Dent, 2006. **9**(2): p. 113-20.
48. Zhang, Y.D., et al., *Kinematics modeling and experimentation of the multi-manipulator tooth-arrangement robot for full denture manufacturing.* J Med Syst, 2011. **35**(6): p. 1421-9.
49. Goodacre, C.J., et al., *CAD/CAM fabricated complete dentures: concepts and clinical methods of obtaining required morphological data.* J Prosthet Dent, 2012. **107**(1): p. 34-46.
50. Kanazawa, M., et al., *Trial of a CAD/CAM system for fabricating complete dentures.* Dent Mater J, 2011. **30**(1): p. 93-6.
51. Inokoshi, M., M. Kanazawa, and S. Minakuchi, *Evaluation of a complete denture trial method applying rapid prototyping.* Dent Mater J, 2012. **31**(1): p. 40-6.
52. Bilgin, M., et al., *Fabricating complete dentures with CAD/CAM and RP technologies.* Journal of Prosthodontics, 2015. **24**.
53. Wimmer, T., et al., *Complete denture fabrication supported by CAD/CAM.* J Prosthet Dent, 2016. **115**(5): p. 541-6.
54. Unkovskiy, A., et al., *Intraoral scanning to fabricate complete dentures with functional borders: a proof-of-concept case report.* BMC Oral Health, 2019. **19**(1): p. 46.
55. Wulfman, C., et al., *Digital removable complete denture: a narrative review.* 2020.
56. Srinivasan, M., et al., *CAD/CAM milled removable complete dentures: time and cost estimation study.* J Dent, 2019. **80**: p. 75-79.
57. Goodacre, B.J., et al., *Comparison of denture base adaptation between CAD-CAM and conventional fabrication techniques.* J Prosthet Dent, 2016. **116**(2): p. 249-56.
58. Srinivasan, M., et al., *CAD/CAM milled removable complete dentures: an in vitro evaluation of trueness.* Clin Oral Investig, 2017. **21**(6): p. 2007-2019.

59. Kalberer, N., et al., *CAD-CAM milled versus rapidly prototyped (3D-printed) complete dentures: An in vitro evaluation of trueness.* J Prosthet Dent, 2019. **121**(4): p. 637-643.
60. AlHelal, A., et al., *Comparison of retention between maxillary milled and conventional denture bases: A clinical study.* J Prosthet Dent, 2017. **117**(2): p. 233-238.
61. AlRumaih, H.S., et al., *Effects of denture adhesive on the retention of milled and heat-activated maxillary denture bases: A clinical study.* J Prosthet Dent, 2018. **120**(3): p. 361-366.
62. Srinivasan, M., et al., *CAD/CAM milled complete removable dental prostheses: An in vitro evaluation of biocompatibility, mechanical properties, and surface roughness.* Dent Mater J, 2018. **37**(4): p. 526-533.
63. Ayman, A.D., *The residual monomer content and mechanical properties of CAD\CAM resins used in the fabrication of complete dentures as compared to heat cured resins.* Electron Physician, 2017. **9**(7): p. 4766-4772.
64. Alp, G., W.M. Johnston, and B. Yilmaz, *Optical properties and surface roughness of prepolymerized poly(methyl methacrylate) denture base materials.* J Prosthet Dent, 2019. **121**(2): p. 347-352.
65. Logozzo, S., et al., *Recent advances in dental optics – Part I: 3D intraoral scanners for restorative dentistry.* Optics and Lasers in Engineering, 2014. **54**: p. 203–221.
66. Kurbad, A., *Impression-free production techniques.* International journal of computerized dentistry, 2011. **14**: p. 59-66.
67. Bosniac, P., P. Rehmann, and B. Wöstmann, *Comparison of an indirect impression scanning system and two direct intraoral scanning systems in vivo.* Clin Oral Investig, 2019. **23**(5): p. 2421-2427.
68. Rudolph, H., et al., *Accuracy of intraoral and extraoral digital data acquisition for dental restorations.* Journal of Applied Oral Science, 2016. **24**: p. 85-94.
69. Kuhr, F., et al., *A new method for assessing the accuracy of full arch impressions in patients.* J Dent, 2016. **55**: p. 68-74.
70. Gimenez-Gonzalez, B., et al., *An In Vitro Study of Factors Influencing the Performance of Digital Intraoral Impressions Operating on Active Wavefront Sampling Technology with Multiple Implants in the Edentulous Maxilla.* J Prosthodont, 2017. **26**(8): p. 650-655.
71. Abduo, J. and M. Elseyoufi, *Accuracy of Intraoral Scanners: A Systematic Review of Influencing Factors.* Eur J Prosthodont Restor Dent, 2018. **26**(3): p. 101-121.
72. van der Meer, W.J., et al., *Application of intra-oral dental scanners in the digital workflow of implantology.* PLoS One, 2012. **7**(8): p. e43312.
73. Richert, R., et al., *Intraoral Scanner Technologies: A Review to Make a Successful Impression.* J Healthc Eng, 2017. **2017**: p. 8427595.
74. Mada, S., et al., *Overview of passive and active vision techniques for hand-held 3D data acquistion.* Proc SPIE, 2003. **39**.
75. Boeddinghaus, M., *Vergleichsstudie zur Genauigkeit von intraoralen optischen Abformungen und einem konventionellen Abformmaterial (Dissertation).* 2014.
76. Anh, J.-w., et al., *A comparison of the precision of three-dimensional images acquired by 2 digital intraoral scanners: Effects of tooth irregularity and scanning direction.* The Korean Journal of Orthodontics, 2016. **46**: p. 3.

77. Marques, S., et al., *Digital Impressions in Implant Dentistry: A Literature Review.* International Journal of Environmental Research and Public Health, 2021. **18**.
78. Ender, A. and A. Mehl, *Influence of scanning strategies on the accuracy of digital intraoral scanning systems.* Int J Comput Dent, 2013. **16**(1): p. 11-21.
79. Medina, P. and A. Pascual, *Accuracy of four digital scanners according to scanning strategy in complete-arch impressions.* PLOS ONE, 2018. **13**.
80. Passos, L., et al., *Impact of different scanning strategies on the accuracy of two current intraoral scanning systems in complete-arch impressions: an in vitro study.* Int J Comput Dent, 2019. **22**(4): p. 307-319.
81. Yilmaz, H., et al., *Effect of Impression Technique and Operator Experience on Impression Time and Operator-Reported Outcomes.* Journal of prosthodontics : official journal of the American College of Prosthodontists, 2021.
82. Müller, P., et al., *Impact of digital intraoral scan strategies on the impression accuracy using the TRIOS Pod scanner.* Quintessence international (Berlin, Germany : 1985), 2016. **47**.
83. Fiore, A., et al., *Influence Of Three Different Scanning Techniques In Full-Arch Implants Digital Impression Using Intraoral Scanners: A Randomized Controlled Cross-Over Trial.* Euras Journal of Health, 2021. **1**: p. 37-50.
84. Patzelt, S.B., et al., *Assessing the feasibility and accuracy of digitizing edentulous jaws.* J Am Dent Assoc, 2013. **144**(8): p. 914-20.
85. Zarone, F., et al., *Comparison of different intraoral scanning techniques on the completely edentulous maxilla: An in vitro 3-dimensional comparative analysis.* Journal of Prosthetic Dentistry, 2020.
86. Kim, J.-E., et al., *Accuracy of intraoral digital impressions using an artificial landmark.* The Journal of Prosthetic Dentistry, 2017. **117**(6): p. 755-761.
87. Fang, J.H., et al., *Digital intraoral scanning technique for edentulous jaws.* J Prosthet Dent, 2018. **119**(5): p. 733-735.
88. Lee, J.-H., *Improved digital impressions of edentulous areas.* The Journal of Prosthetic Dentistry, 2017. **117**(3): p. 448-449.
89. Flügge, T.V., et al., *Precision of intraoral digital dental impressions with iTero and extraoral digitization with the iTero and a model scanner.* Am J Orthod Dentofacial Orthop, 2013. **144**(3): p. 471-8.
90. Guth, J.F., et al., *Accuracy of digital models obtained by direct and indirect data capturing.* Clin Oral Investig, 2013. **17**(4): p. 1201-8.
91. Malik, J., et al., *Comparison of Accuracy Between a Conventional and Two Digital Intraoral Impression Techniques.* Int J Prosthodont, 2018. **31**(2): p. 107-113.
92. Nedelcu, R., et al., *Accuracy and precision of 3 intraoral scanners and accuracy of conventional impressions: A novel in vivo analysis method.* J Dent, 2018. **69**: p. 110-118.
93. Hack, G., et al., *Computerized optical impression making of edentulous jaws - An in vivo feasibility study.* J Prosthodont Res, 2020.
94. Tasaka, A., et al., *Applying intraoral scanner to residual ridge in edentulous regions: In vitro evaluation of inter-operator validity to confirm trueness.* BMC Oral Health, 2019. **19**.
95. Braian, M. and A. Wennerberg, *Trueness and precision of 5 intraoral scanners for scanning edentulous and dentate complete-arch mandibular*

casts: A comparative in vitro study. J Prosthet Dent, 2019. **122**(2): p. 129-136 e2.
96. Iturrate, M., H. Eguiraun, and E. Solaberrieta, *Accuracy of digital impressions for implant-supported complete-arch prosthesis, using an auxiliary geometry part-An in vitro study.* Clin Oral Implants Res, 2019. **30**(12): p. 1250-1258.
97. Iturrate, M., et al., *Accuracy analysis of complete-arch digital scans in edentulous arches when using an auxiliary geometric device.* J Prosthet Dent, 2019. **121**(3): p. 447-454.
98. Andriessen, F.S., et al., *Applicability and accuracy of an intraoral scanner for scanning multiple implants in edentulous mandibles: a pilot study.* J Prosthet Dent, 2014. **111**(3): p. 186-94.
99. Fang, J.H., et al., *Development of complete dentures based on digital intraoral impressions-Case report.* J Prosthodont Res, 2018. **62**(1): p. 116-120.
100. Goodacre, B.J. and C.J. Goodacre, *Using Intraoral Scanning to Fabricate Complete Dentures: First Experiences.* Int J Prosthodont, 2018. **31**(2): p. 166-170.
101. Goodacre, B.J., C.J. Goodacre, and N.Z. Baba, *Using Intraoral Scanning to Capture Complete Denture Impressions, Tooth Positions, and Centric Relation Records.* Int J Prosthodont, 2018. **31**(4): p. 377-381.
102. Lo Russo, L. and A. Salamini, *Single-arch digital removable complete denture: A workflow that starts from the intraoral scan.* J Prosthet Dent, 2018. **120**(1): p. 20-24.
103. Lo Russo, L., et al., *Digital dentures: A protocol based on intraoral scans.* J Prosthet Dent, 2021. **125**(4): p. 597-602.
104. Schimmel, M., et al., *Accuracy of intraoral scanning in completely and partially edentulous maxillary and mandibular jaws: an in vitro analysis.* Clin Oral Investig, 2021. **25**(4): p. 1839-1847.
105. Tasaka, A., et al., *Applying intraoral scanner to residual ridge in edentulous regions: in vitro evaluation of inter-operator validity to confirm trueness.* BMC Oral Health, 2019. **19**(1): p. 264.
106. Osnes, C.A., et al., *Full arch precision of six intraoral scanners in vitro.* J Prosthodont Res, 2020. **64**(1): p. 6-11.
107. Jung, S., et al., *Comparison of different impression techniques for edentulous jaws using three-dimensional analysis.* J Adv Prosthodont, 2019. **11**(3): p. 179-186.
108. Lo Russo, L., et al., *Three-dimensional differences between intraoral scans and conventional impressions of edentulous jaws: A clinical study.* J Prosthet Dent, 2020. **123**(2): p. 264-268.
109. Chebib, N., et al., *Edentulous jaw impression techniques: An in vivo comparison of trueness.* J Prosthet Dent, 2019. **121**(4): p. 623-630.
110. Gutmacher, Z., et al., *Evaluation of the accuracy of multiple digital impression systems on a fully edentulous maxilla.* Quintessence Int, 2021. **52**(6): p. 488-495.
111. Alkhodary, M., *Optical versus conventional impressions of the completely edentulous arches.* Egyptian Dental Journal, 2021. **67**: p. 1407-1415.
112. Cao, Y., et al., *[Accuracy of three intraoral scans for primary impressions of edentulous jaws].* Beijing Da Xue Xue Bao Yi Xue Ban, 2020. **52**(1): p. 129-137.

113. Rasaie, V., J. Abduo, and S. Hashemi, *Accuracy of Intraoral Scanners for Recording the Denture Bearing Areas: A Systematic Review.* J Prosthodont, 2021.
114. O'Toole, S., et al., *Investigation into the accuracy and measurement methods of sequential 3D dental scan alignment.* Dent Mater, 2019. **35**(3): p. 495-500.
115. Guth, J.F., et al., *A new method for the evaluation of the accuracy of full-arch digital impressions in vitro.* Clin Oral Investig, 2016. **20**(7): p. 1487-94.
116. Schmidt, A., et al., *Torsion and linear accuracy in intraoral scans obtained with different scanning principles.* J Prosthodont Res, 2020. **64**(2): p. 167-174.
117. Kim, R.J.Y., G.I. Benic, and J.M. Park, *Trueness of ten intraoral scanners in determining the positions of simulated implant scan bodies.* Sci Rep, 2021. **11**(1): p. 2606.
118. Kim, K.R., K.Y. Seo, and S. Kim, *Conventional open-tray impression versus intraoral digital scan for implant-level complete-arch impression.* J Prosthet Dent, 2019. **122**(6): p. 543-549.
119. Kontis, P., et al., *Accuracy of intraoral scans of edentulous jaws with different generations of intraoral scanners compared to laboratory scans.* J Adv Prosthodont, 2021. **13**(5): p. 316-326.
120. Mahmood, D., et al., *Trueness and Precision of Three-Dimensional Digitizing Intraoral Devices.* International Journal of Dentistry, 2018. **2018**.
121. Braian, M. and A. Wennerberg, *Trueness and precision of 5 intraoral scanners for scanning edentulous and dentate complete-arch mandibular casts: A comparative in vitro study.* J Prosthet Dent, 2019.
122. Ciocca, L., et al., *In vitro assessment of the accuracy of digital impressions prepared using a single system for full-arch restorations on implants.* Int J Comput Assist Radiol Surg, 2018. **13**(7): p. 1097-1108.
123. Mandelli, F., et al., *Full-arch intraoral scanning: Comparison of two different strategies and their accuracy outcomes.* Journal of Osseointegration, 2018. **10**: p. 65-74.
124. Mangano, F.G., et al., *Trueness of 12 intraoral scanners in the full-arch implant impression: a comparative in vitro study.* BMC Oral Health, 2020. **20**(1): p. 263.
125. Gintaute, A., et al., *Accuracy of computerized and conventional impression-making procedures for multiple straight and tilted dental implants.* Int J Esthet Dent, 2018. **13**(4): p. 550-565.
126. Iturrate, M., et al., *Accuracy analysis of complete-arch digital scans in edentulous arches when using an auxiliary geometric device.* J Prosthet Dent, 2018.
127. Gimenez, B., et al., *Accuracy of a digital impression system based on parallel confocal laser technology for implants with consideration of operator experience and implant angulation and depth.* Int J Oral Maxillofac Implants, 2014. **29**(4): p. 853-62.
128. Fukazawa, S., C. Odaira, and H. Kondo, *Investigation of accuracy and reproducibility of abutment position by intraoral scanners.* J Prosthodont Res, 2017. **61**(4): p. 450-459.
129. Renne, W., et al., *Evaluation of the accuracy of 7 digital scanners: An in vitro analysis based on 3-dimensional comparisons.* J Prosthet Dent, 2017. **118**(1): p. 36-42.
130. Schmidt, A., et al., *Accuracy of Digital and Conventional Full-Arch Impressions in Patients: An Update.* J Clin Med, 2020. **9**(3).

131. Runkel, C., et al., *Digital impressions in dentistry-accuracy of impression digitalisation by desktop scanners.* Clin Oral Investig, 2020. **24**(3): p. 1249-1257.
132. Peng, L., et al., *Accuracy and reproducibility of virtual edentulous casts created by laboratory impression scan protocols.* J Prosthet Dent, 2018. **120**(3): p. 389-395.
133. Persson, A.S., et al., *Digitization of simulated clinical dental impressions: virtual three-dimensional analysis of exactness.* Dent Mater, 2009. **25**(7): p. 929-36.
134. DeLong, R., et al., *Factors influencing optical 3D scanning of vinyl polysiloxane impression materials.* J Prosthodont, 2001. **10**(2): p. 78-85.
135. Chebib, N., et al., *Edentulous jaw impression techniques: An in vivo comparison of trueness.* J Prosthet Dent, 2018.
136. Kim, K.R., K.Y. Seo, and S. Kim, *Conventional open-tray impression versus intraoral digital scan for implant-level complete-arch impression.* J Prosthet Dent, 2019.
137. Revilla-León, M., et al., *Comparison of conventional, photogrammetry, and intraoral scanning accuracy of complete-arch implant impression procedures evaluated with a coordinate measuring machine.* The Journal of Prosthetic Dentistry, 2021. **125**(3): p. 470-478.
138. Gimenez Gonzalez, B., et al., *Accuracy of a Digital Impression System Based on Parallel Confocal Laser Technology for Implants with Consideration of Operator Experience and Implant Angulation and Depth.* The International journal of oral & maxillofacial implants, 2014. **29**: p. 853-862.
139. FinoGmbH, *FINO SCAN STONE Technisches Datenblatt.* 10044, 2015.
140. Piwowarczyk, A., et al., *In vitro study on the dimensional accuracy of selected materials for monophase elastic impression making.* Int J Prosthodont, 2002. **15**(2): p. 168-74.
141. Imburgia, M., et al., *Accuracy of four intraoral scanners in oral implantology: a comparative in vitro study.* BMC Oral Health, 2017. **17**(1): p. 92.
142. Carlsson, G.E., A. Ortorp, and R. Omar, *What is the evidence base for the efficacies of different complete denture impression procedures? A critical review.* J Dent, 2013. **41**(1): p. 17-23.
143. Kattadiyil, M.T., et al., *Intraoral scanning of hard and soft tissues for partial removable dental prosthesis fabrication.* J Prosthet Dent, 2014. **112**(3): p. 444-8.
144. Saygılı, S., O. Geckili, and T. Sulun, *Prosthetic Rehabilitation of an Edentulous Patient with Microstomia Using Both Digital and Conventional Techniques: A Clinical Report.* J Prosthodont, 2019. **28**(5): p. 488-492.
145. Wu, J., Y. Li, and Y. Zhang, *Use of intraoral scanning and 3-dimensional printing in the fabrication of a removable partial denture for a patient with limited mouth opening.* The Journal of the American Dental Association, 2017. **148**.

8. Summary

This study evaluated the trueness and precision of direct digitization and indirect digitization of an edentulous maxilla.

An edentulous jaw model made of PEEK, featuring four hemispherical geometries on the alveolar ridge, served as the testing model. The PEEK model was industrially digitized to obtain a reference dataset (REF). Subsequently, the model was digitized according to the clinical workflow (n=25/group) with the following IOS: Cerec Primescan AC (PRI); Trios 3 Wireless (TRS); True Definition (TRD); iTero Element (ITE); Cerec AC Omnicam (OMN). In addition, conventional impressions were taken with scannable PVS (Flexitime Fast&Scan light flow and Flexitime Monophase Pro Scan) and scanned (n=25/group) with laboratory scanners: D810 (D8I) and In EOS X5 (E5I). The impressions were poured, and the resulting stone casts were scanned (n=25/group) with D810 (D8M) and In EOS X5 (E5M). Linear and angular parameters were measured in the virtual model data and compared to REF.

One-way ANOVA detected significant differences for all tested parameters. The highest trueness in the P17-P13 and the P17-P23 distances was revealed by group E5I, and in the P17-P27 distance by group PRI. Regarding angular parameters in the transverse plane group, D8M showed the best trueness with no significant difference to any other group, while in the sagittal plane E5M exhibited the highest trueness. Group D8I was most precise in all linear parameters and angle XZ, while group E5I exhibited the highest precision in angle YZ.

Digitization of conventional impressions presented the most accurate results. PRI demonstrated values similar to impression digitization and superior to stone cast digitization, while TRS and OMN performed similarly to stone cast digitization.

9. Zusammenfassung

Diese Studie bewertete die Richtigkeit und Präzision direkter und indirekter Digitalisierung eines zahnlosen Oberkiefers. Als Testmodell diente ein zahnloses Oberkiefermodell aus PEEK mit vier halbkugelförmigen Geometrien am Kieferkamm. Das PEEK-Modell wurde industriell digitalisiert, um einen Referenzdatensatz (REF) zu erhalten. Anschließend wurde das Modell mit folgendem IOS digitalisiert (n=25/Gruppe): Cerec Primescan AC (PRI); Trios 3 Wireless (TRS); True Definition (TRD); iTero-Element (ITE); Cerec AC Omnicam (OMN). Darüber hinaus wurden konventionelle Abformungen mit scanbarem PVS (Flexitime Fast&Scan light flow und Flexitime Monophase Pro Scan) aufgenommen und mit Laborscannern: D810 (D8I) und In EOS X5 (E5I) gescannt (n=25/Gruppe). Die Abformungen wurden gegossen und die resultierenden Gipsmodelle wurden gescannt (n=25/Gruppe) mit: D810 (D8M) und In EOS X5 (E5M). Lineare und Winkelparameter wurden gemessen und mit REF verglichen. Die Einfaktorielle-ANOVA stellte signifikante Unterschiede für alle getesteten Parameter fest. Die höchste Richtigkeit in den Distanzen P17-P13 und P17-P23 wurde von Gruppe E5I und in der Distanz P17-P27 von Gruppe PRI gezeigt. Hinsichtlich der Winkelparameter in der transversalen Ebene zeigte Gruppe D8M die beste Richtigkeit ohne signifikanten Unterschied zu anderen Gruppen, während E5M in der Sagittalebene die höchste Richtigkeit aufwies. Gruppe D8I war in allen linearen Parametern und im Winkel XZ am präzisesten, während Gruppe E5I die höchste Präzision im Winkel YZ aufwies. Die Digitalisierung konventioneller Abformungen lieferte die genauesten Ergebnisse. PRI zeigte ähnliche Werte zur Digitalisierung von Abformungen und war der Digitalisierung von Gipsmodellen überlegen, während TRS und OMN ähnliche Leistungen wie die Digitalisierung von Gipsmodellen zeigten.

10. Appendix

10.1 List of Tables

10.2 List of Figures

11. List of Abbreviations

CAD/CAM	Computer-aided design/ Computer-aided manufacture
IOS	Intraoral scanner
EOS	Extraoral scanner
PVS	Polyvinyl siloxane
VPS	Vinyl polysiloxan
PVES	Polyvinyl Ether Silicone
CNC	Computer numerical control
3D	Three-dimensional
CCD	Charge-coupled device
CMOS	Complementary metal-oxide semiconductor
AWS	Active wavefront sampling
TiO_2	Titanium dioxide
STL	Surface tessellation language
PEEK	Polyether ether ketone
REF	Reference dataset
ANOVA	Analysis of variance
SD	Standard deviation
CI	Confidence Interval

12. Acknowledgements

I would like to thank Professor Dr. Daniel Edelhoff, director of the Polyclinic for Dental Prosthetics at the Ludwig Maximilian University in Munich, for giving me the opportunity to write the doctoral thesis.

I wish to express my gratitude to my supervisor Prof. Dr. Jan-Frederik Güth for suggesting the topic of the doctoral thesis and his competent guidance.

I would also like to sincerely thank PD Dr. med. dent. Christine Keul for her patience, constructive and friendly support during the writing of my doctoral thesis, and her help with data analysis and statistics.

I would also like to extend a warm thank you to Dr. rer. biol. hum. Dipl. Ing. Kurt Erdelt for designing the dataset for the testing model.

Moreover, I wish to express my appreciation to Josef Schweiger, director of the laboratory of the Polyclinic for Dental Prosthetics, for his assistance with the fabrication of the testing model and the extraoral laboratory scanners.

I would like to express my gratitude to my partner Thea for her support and motivation during my doctorate.

Finally, I would also like to thank my parents for their encouragement.

13. Affidavit

Eidesstattliche Versicherung

_____

Ich, Panagiotis Kontis erkläre hiermit an Eides statt, dass ich die vorliegende Dissertation mit dem Titel:

"Analysis of digitization methods for edentulous jaws"

selbständig verfasst, mich außer der angegebenen keiner weiteren Hilfsmittel bedient und alle Erkenntnisse, die aus dem Schrifttum ganz oder annähernd übernommen sind, als solche kenntlich gemacht und nach ihrer Herkunft unter Bezeichnung der Fundstelle einzeln nachgewiesen habe.

Ich erkläre des Weiteren, dass die hier vorgelegte Dissertation nicht in gleicher oder in ähnlicher Form bei einer anderen Stelle zur Erlangung eines akademischen Grades eingereicht wurde.

Panagiotis Kontis

München, den 30.05.2023

14. List of Publications

Parts of this dissertation are included in the following publication:

Kontis P, Güth JF, Schubert O, Keul C. Accuracy of intraoral scans of edentulous jaws with different generations of intraoral scanners compared to laboratory scans. J Adv Prosthodont. 2021;13(5):316-326. doi:10.4047/jap.2021.13.5.316